

Article

A Comparison of β -Phenyl Elimination in Nickel and Palladium Alkyl Complexes: A Potentially Relevant Process in the Mizoroki–Heck Reaction

Jorge A. López, Diego A. Cabo, Pilar Palma and Juan Cámpora * 

Instituto de Investigaciones Químicas, CSIC—Universidad de Sevilla, Centro de Investigaciones Científicas “Isla de la Cartuja”, C/Américo Vespucio, 49, 41092 Sevilla, Spain; albinol@ugto.mx (J.A.L.); diego.cabo@iiq.csic.es (D.A.C.); ppalma@iiq.csic.es (P.P.)

* Correspondence: campora@iiq.csic.es

Abstract: There is currently much interest in avoiding precious metals in catalysis. The development of nickel catalysts to replace palladium in the Mizoroki–Heck reaction is a relevant case in this line of research, since both elements share many chemical features. This contribution focuses on β -phenyl (β -Ph) elimination in alkyl–nickel complexes. This is the microscopic reverse of olefin insertion (or carbometallation), a fundamental step in the Heck cycle that is usually considered irreversible and selectivity-determining. However, the potential reversibility of carbometallation is generally concealed by the facile β -hydrogen (β -H) elimination that follows. Where β -hydrogen elimination is hindered, β -aryl elimination may ensue. We have previously shown that cationic 2-methyl-2-phenylpropyl (neophyl) palladium complexes supported by bidentate ligands experience β -Ph elimination, which can be seen as an example of olefin de-insertion. In this contribution, we report that β -Ph elimination can also occur in their nickel analogs, in which case fast hydrolyses of the resulting phenyl product can follow the reaction. We investigated the mechanism of these processes and compared their feasibility for nickel and palladium catalysts using DFT calculations. These results are relevant information for the design of nickel-based catalysts for the Heck reaction.

Keywords: β -carbon elimination; olefin insertion; Mizoroki–Heck reaction; nickel; palladium



Citation: López, J.A.; Cabo, D.A.; Palma, P.; Cámpora, J. A Comparison of β -Phenyl Elimination in Nickel and Palladium Alkyl Complexes: A Potentially Relevant Process in the Mizoroki–Heck Reaction. *Inorganics* **2024**, *12*, 89. <https://doi.org/10.3390/inorganics12030089>

Academic Editors: Axel Klein, S. Masoud Nabavizadeh and Fatemeh Niroomand Hosseini

Received: 21 February 2024

Revised: 8 March 2024

Accepted: 11 March 2024

Published: 14 March 2024

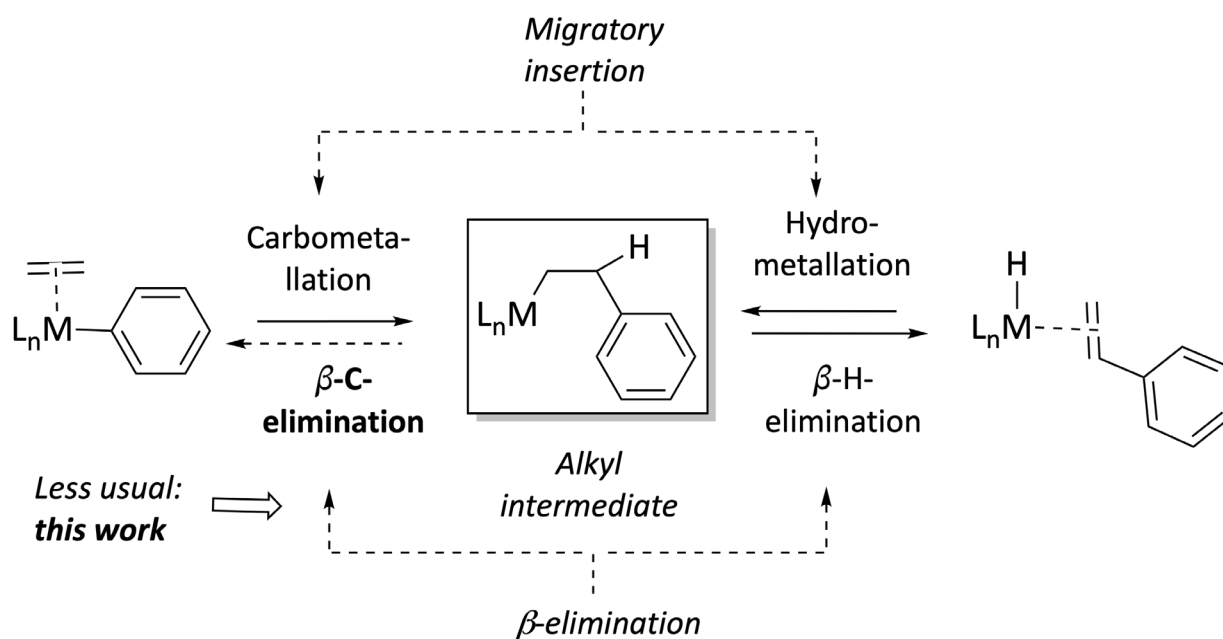


Copyright: © 2024 by the authors. Licensee MDPI, Basel, Switzerland. This article is an open access article distributed under the terms and conditions of the Creative Commons Attribution (CC BY) license (<https://creativecommons.org/licenses/by/4.0/>).

1. Introduction

Olefin insertion into metal–carbon bonds, or olefin carbometallation, is a fundamental process responsible for C–C bond formation in valuable catalytic processes [1], such as olefin polymerization [2–12] and oligomerization [13–19], or the Mizoroki–Heck reaction [20,21]. In most cases, this involves a migratory insertion route. This mechanistic category implies the pre-coordination of the olefin molecule to the metal center, followed by the attack by a pre-existing σ bonded ligand (Scheme 1) [1]. The reversal of olefin insertion into a metal–carbon bond is called β -carbon (β -C) elimination. Although the microscopic reversibility principle [22] dictates that the latter should also occur, this is much more rarely observed [23].

In contrast, β -hydrogen (β -H) elimination, the reverse of olefin insertion into metal–hydride bonds (hydrometallation), is ubiquitous. In part, the difference stems from thermodynamic reasons. Usually, β -C elimination is endothermic since the formation of an olefin π -bond does not compensate for the cleavage of a strong σ C–C bond [24]. In contrast, for β -H elimination, the strength of the M–H bond compensates for this unfavorable factor, leading to a nearly thermoneutral balance on a general basis. The literature collects many examples of reversible β -H elimination [5,25–30]. Kinetic reasons also play a critical part in the scarcity of β -C eliminations: there are usually more C–H bonds in β positions, which are much more readily accessible for the metal than β -C–C bonds. In addition, the interaction of the metal with a C–C bond implies the reorganization of highly directional atomic p orbitals of carbon, in contrast with the non-directional s orbital of the hydrogen atom [31].



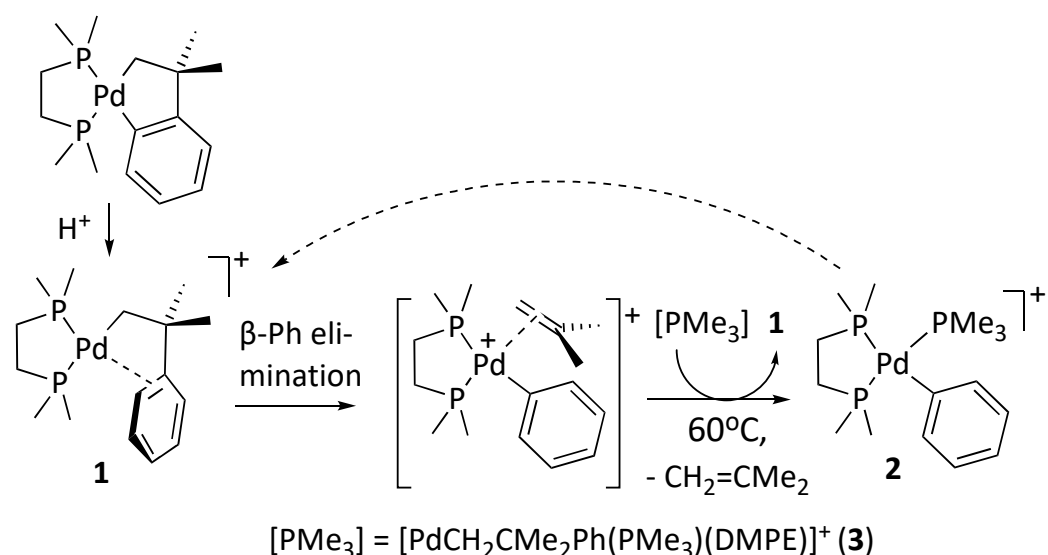
Scheme 1. Migratory olefin insertion into M–C (carbometallation, left) and M–H bonds (hydrometallation, right) and their reverse processes, β -C and β -H elimination.

In the Mizoroki–Heck reaction, olefin insertion produces organic fragments with one or more C–H bonds. Therefore, the potential reversibility of the olefin insertion reaction is usually masked by competitive β -H elimination. The prevalence of β -H over β -C eliminations is an essential feature of the Mizoroki–Heck reaction, where olefin carbometallation is followed by fast β -H elimination.

Despite the above considerations, β -C elimination is an accessible mechanistic avenue that emerges as a dominant process in some situations. For instance, β -methyl elimination constitutes a frequent termination mechanism in propene polymerization by early transition metals, for which the process becomes exergonic due to the increased strength of the resulting M–Me bond [32]. Very recently, a Hf(IV) metallocene/MAO catalyst has even been shown to depolymerize polypropylene, which implicitly involves the ability to revert the propene enchainment reaction via β -alkyl elimination recursively [33]. Although the thermodynamic preference of transition metals for β -hydrogen over β -carbon elimination increases as the metal center becomes electron-richer along the transition rows [22], alkyl–metal complexes of palladium and platinum experience β -carbon elimination if favorable conditions are met. For instance, β -C prevails over β -H eliminations if it involves strained, reactive C–C bonds, such as those in cyclopropane or cyclobutane, or when a rigid configuration of the alkyl ligand prevents C–H bonds in the β -position to attain a coplanar arrangement with the metal fragment, as required to enable β -H elimination [34]. Reversible olefin insertion is involved in the Catellani reaction (palladium–norbornene cooperative catalysis), in which norbornene insertion and de-insertion into Pd–aryl bonds enables the functionalization of the aryl ring on both ortho positions via cascade-type insertion–cyclometallation–alkylation reactions [35]. Interestingly, Amatore and Jutand proposed that reversible olefin insertions may play a role in the regioselectivity control of the Mizoroki–Heck reaction of electron-rich olefins under cationic conditions when cationic Pd/diphosphine complexes catalyze the arylation [36]. This implies that, in such cases, the energy barriers for β -phenyl (β -Ph) and β -H eliminations are comparable.

Years ago, our group [37] and others [38] reported that alkyl ligands with a β -phenyl group can stabilize formally unsaturated 14-electron Pd species such as **1** owing to their ability to donate π -electrons to the electron-deficient metal center (Scheme 2). In this work, we used the neophyl group (i.e., 2-methyl-2-phenylpropyl), as a privileged platform for investigating β -Ph elimination. This alkyl group contains no β -H atoms, fea-

turing only methyl and phenyl substituents, and any β -carbon elimination occurs without raising the reactivity of the C–C bonds with ring strain. Depending on the spectator co-ligands, such π -arene interactions serve as precursors for various reactions, mainly o -metallation or β -Ph elimination. Specifically, whereas monodentate PMe_3 ligands favor o -phenyl palladation [37], the electronically similar but chelating diphosphine 1,2-bis(dimethylphosphino)ethane (DMPE) selectively induces β -Ph elimination (Scheme 2) [39]. To stabilize the Pd(II)–Ph product as the PMe_3 adduct **2**, the coordinatively saturated neophyl complex $[\text{Pd}(\text{CH}_2\text{CMe}_2\text{Ph})(\text{PMe}_3)(\text{DMPE})]^+ [\text{BAr}'_4]^-$ (**3**, $\text{Ar}' = 3,5$ -bistrifluoromethylphenyl) is used as a PMe_3 source. Compound **3** is not reactive by itself: it requires the presence of **1**, which is responsible for the β -Ph elimination process. Such reaction sequence ultimately leads to a **1**-catalyzed conversion of **3** into **2**, concurrent with isobutene elimination. The resistance of the saturated, 16-electron complex **3** to β -Ph elimination stands in contrast with the ability of palladium alkyl complexes susceptible to the β -H elimination process, which is known to proceed even from either 14- or 16-electron alkyl intermediates [39]. The latter involves a pentacoordinate transition state for the hydrogen abstraction, in accordance with early computational work by Thorn and Hoffmann [40]. As commented above, the reluctance of palladium alkyls to undergo β -carbon through pentacoordinate intermediates contrasts with their ability for β -H elimination. This feature is paramount for the efficiency and selectivity of the Mizoroki–Heck reaction.



Scheme 2. Previous results demonstrating β -Ph elimination in the Pd π -arene complex **1**. The otherwise stable complex **3** is used as a PMe_3 source.

In this contribution, we report on the ability of cationic neophyl Ni(II) species akin to the above Pd(II) complexes to undergo β -Ph elimination. We provide evidence for β -Ph elimination from Ni(II) complexes under mild conditions for the first time. Whereas β -C elimination reactions are not alien to Ni(II) chemistry [41,42], to our knowledge, this has never been noted for non-strained complexes. Surprisingly, Ni(II) phenyl complexes arising from the isobutene de-insertion are exceedingly prone to hydrolysis, being converted into binuclear hydroxides by the moisture traces in reagents, solvents, and equipment.

Due to the potential importance that the reversibility of olefin insertion may have for the applications of Ni as a more sustainable replacement for Pd in homogeneous catalysis, we complete this study with a comparative computational analysis of β -Ph elimination in 14- and 16-electron complexes of Ni(II) and Pd(II). Our studies include the final hydrolyses step, as this could represent an essential difference in the stability of both types of catalysts.

2. Materials and Methods

General Considerations. All experiments were carried out under dry nitrogen using standard Schlenk techniques. Solvents were rigorously dried and degassed before use. Microanalyses were performed by Pascher Microanalytical Laboratory (Remagen, Germany) and the Microanalytical Service of the University of Seville and Instituto de Investigaciones Químicas (Seville, Spain). Infrared spectra were recorded in Nujol mulls on Perkin-Elmer FT-16PC (Shelton, CT, USA) and Bruker Vector 22 spectrometers (Bruker Optics, Ettlingen, Germany) while NMR spectra were obtained on Bruker AMX-300, AMX-500, DRX-400, and DRX-500 spectrometers (Bruker AXS, Karlsruhe, Germany). $^{31}\text{P}\{^1\text{H}\}$ NMR resonances are referenced to 85% H_3PO_4 as an external standard. The residual ^1H and $^{13}\text{C}\{^1\text{H}\}$ resonances of the solvents were used as internal standards, but the chemical shifts were reported relative to TMS. Chemical shifts (δ) are given in ppm, and coupling constants (J) are given in Hz. Abbreviations for multiplicities are as follows: br, broad; s, singlet; d, doublet; t, triplet; c, quartet; q, quintet; sp, septet; m, multiplet; v, virtual; dvt, doublet of virtual triplet; pt, pseudo triplet. Compounds **4a,b** [43], $[\text{Ni}(\text{Me})_2\text{DiPP}]$ [43], and $[\text{HPMe}_3][\text{BAr}'_4]$ [39] were prepared as reported previously. Pyridinium triflate was prepared as a white precipitate by mixing equimolar amounts of triflic acid and pyridine in diethyl ether, which was filtered and dried under vacuum.

$[\text{Ni}(\text{OH})\text{DiPPE}]_2[\text{TfO}]_2$, **5a**, and $[\text{Ni}(\text{OH})\text{DiPPP}]_2[\text{TfO}]_2$, **5b**. 0.78 mL of a 0.64 M solution of HTfO (0.5 mmol) in Et_2O was added to a stirred solution of complex **4a** (226 mg, 0.5 mmol) in 30 mL of Et_2O at -80°C . The resulting yellow suspension was allowed to reach room temperature and then stirred at room temperature for one hour. The suspension turned to a red-orange color. This was evaporated to dryness, and the residue was extracted with 20 mL of CH_2Cl_2 . The solution was filtered and concentrated under reduced pressure, and some toluene was added. Compound **5a** was obtained as red crystals after cooling the solution in the freezer at -30°C . (Yield: 88%.) Anal. Calcd. for $\text{C}_{30}\text{H}_{66}\text{F}_6\text{Ni}_2\text{O}_8\text{P}_4\text{S}_2 \cdot 0.5\text{C}_7\text{H}_8$: C, 39.44; H, 6.92. Found: C, 38.90; H, 7.14. IR (Nujol mull): $\nu(\text{O-H})$ 3594 cm^{-1} . ^1H NMR (400 MHz, CD_2Cl_2 , 25°C): δ -1.51 (q, 1H, $J_{\text{HP}} = 1.9\text{ Hz}$, OH), 1.25 (dd, 12H, $^3J_{\text{HP}} = 13.9\text{ Hz}$, $^3J_{\text{HH}} = 7.0\text{ Hz}$, CH_3), 1.56 (d, 4H, $J_{\text{HP}} = 11.3\text{ Hz}$, CH_2), 1.67 (dd, 12H, $^3J_{\text{HP}} = 17.9\text{ Hz}$, $^3J_{\text{HH}} = 7.0\text{ Hz}$, CH_3), 2.38 (m, 4H, CH). $^{13}\text{C}\{^1\text{H}\}$ NMR (100.6 MHz, CD_2Cl_2 , 25°C): δ 19.6 (s, 4C, CH_3), 20.0 (t, 2C, $J_{\text{CP}}^* = 20.0\text{ Hz}$, CH_2), 22.3 (s, 4C, CH_3), 26.3 (t, 4C, $J_{\text{CP}}^* = 12.0\text{ Hz}$, CH), 122.5 (c, 2C, $^1J_{\text{CF}} = 321.0\text{ Hz}$, CF_3). $^{31}\text{P}\{^1\text{H}\}$ NMR (162 MHz, CD_2Cl_2 , 25°C) δ 88.0 (s).

Compound **5b** was prepared using the same procedure. (Yield: 85%.) Anal. Calcd. for $\text{C}_{32}\text{H}_{70}\text{F}_6\text{Ni}_2\text{O}_8\text{P}_4\text{S}_2$: C, 38.35; H, 7.04. Found: C, 38.37; H, 6.92. IR (Nujol mull): $\nu(\text{O-H})$ 3513 cm^{-1} . ^1H NMR (400 MHz, CD_2Cl_2 , 25°C): δ -3.27 (s, 1H, OH), 1.30 (m, 16H, CH_3 , CH_2) 1.70 (dd, 12H, $^3J_{\text{HP}} = 17.5\text{ Hz}$, $^3J_{\text{HH}} = 8.0\text{ Hz}$, CH_3), 1.83 (m, 2H, CH_2), 2.01 (m, 4H, CH). $^{13}\text{C}\{^1\text{H}\}$ NMR (100.6 MHz, CD_2Cl_2 , 25°C) δ 14.7 (t, 2C, $J_{\text{CP}}^* = 16.0\text{ Hz}$, CH_2), 17.7 (s, 4C, CH_3), 20.7 (s, 1C, CH_2), 20.8 (s, 4C, CH_3), 25.2 (t, 4C, $J_{\text{CP}}^* = 12.0\text{ Hz}$, CH). $^{31}\text{P}\{^1\text{H}\}$ NMR (162 MHz, CD_2Cl_2 , 25°C) δ 27.4 (s).

$\text{Ni}(\text{CH}_2\text{CMe}_2\text{Ph})(\text{TfO})(\text{DiPPE})$, **6a**, and $\text{Ni}(\text{CH}_2\text{CMe}_2\text{Ph})(\text{TfO})(\text{DiPPP})$, **6b**. A solution of the complex **4a** (220 mg, 0.44 mmol) in 50 mL of Et_2O and cooled to -75°C was treated with 0.73 mL (0.44 mmol) of a 0.6 M solution of HTfO in Et_2O . The mixture was stirred for 15 min at this temperature, and a yellow precipitate was formed. The suspension was filtered, and the solid residue was dried under vacuum. ^1H NMR (400 MHz, CD_2Cl_2 , 25°C): δ 0.78 (dd, 2H, $^3J_{\text{HP}} = 4.8, 14.0\text{ Hz}$, Ni- CH_2), 1.35 (m, 16H, CH_3 , CH_2 DiPPE), 1.40 (s, 6H, CMe_2), 1.45 (m, 12H, CH_3 DiPPE), 2.26 (m, 2H, CH DiPPE), 2.39 (m, 2H, CH DiPPE), 7.56 (t, 1H, $^3J_{\text{HH}} = 6.6\text{ Hz}$, $p\text{-CH}_{\text{ar}}$), 7.82 (t, 2H, $^3J_{\text{HH}} = 6.3\text{ Hz}$, $m\text{-CH}_{\text{ar}}$), 8.00 (d, 2H, $^3J_{\text{HH}} = 7.0\text{ Hz}$, $o\text{-CH}_{\text{ar}}$). $^{31}\text{P}\{^1\text{H}\}$ (162 MHz, CD_2Cl_2 , 25°C) AX spin system: $\delta_{\text{A}} = 57.0$, $\delta_{\text{X}} = 69.2$, $^2J_{\text{AX}} = 9.3\text{ Hz}$.

6b: Applying the same procedure to **4b** led to a yellow precipitate, which was similarly collected, and its ^1H and $^{31}\text{P}\{^1\text{H}\}$ spectra were recorded in CD_2Cl_2 . The sample was impurified with **5b**. Therefore, only selected signals are provided. ^1H NMR (400 MHz, CD_2Cl_2 , 25°C): δ $1.2\text{--}1.5$ (DiPPP ligand and Ni- CH_2 , overlapping signals), 1.56 (s, 6H,

CMe_2), 1.72–2.26 (m, 2H, CH DiPPP), 7.20 (t, 1H, $^3J_{\text{HH}} = 6.6$ Hz, $p\text{-CH}_{\text{ar}}$), 7.34 (t, 2H, $^3J_{\text{HH}} = 6.4$ Hz, $m\text{-CH}_{\text{ar}}$), 7.53 (d, 2H, $^3J_{\text{HH}} = 6.0$ Hz, $o\text{-CH}_{\text{ar}}$). $^{31}\text{P}\{^1\text{H}\}$ (162 MHz, CD_2Cl_2 , 25 °C) AX spin system: $\delta_{\text{A}} = 10.3$, $\delta_{\text{X}} = 30.7$ (broad), $^2J_{\text{AX}} = 29.3$ Hz.

$[\text{Ni}(\text{CH}_2\text{CMe}_2\text{Ph})(\text{py})\text{DiPPE}][\text{TfO}]$, **7a**, and $[\text{Ni}(\text{Ph})(\text{py})\text{DiPPE}][\text{TfO}]$, **8a**. A sample of 240 mg (0.5 mmol) of complex **4a** was dissolved in 30 mL of Et_2O , the solution was cooled to -60 °C, and a suspension of 125 mg (0.5 mmol) of pyridinium triflate in 20 mL of Et_2O was added. The mixture was stirred at -20 °C for two hours, forming a yellow solid. The suspension was filtered, and the solid residue dried under a vacuum. A sample was dissolved in CD_2Cl_2 , and NMR spectra were recorded immediately and 24 h later. The former shows mainly signals of **7a** and the latter of **8a**. Data for **7a**: ^1H (400 MHz, CD_2Cl_2 , 25 °C): δ 0.85 (dd, 6H, $^3J_{\text{HP}} = 15.0$ Hz, $^3J_{\text{HH}} = 7.5$ Hz, CH_3 DiPPE), 1.05 (dd, 6H, $^3J_{\text{HP}} = 12.7$ Hz, $^3J_{\text{HH}} = 6.9$ Hz, CH_3 DiPPE), 1.25 (s, 6H, CMe_2), 1.38 (dd, 6H, $^3J_{\text{HP}} = 13.7$ Hz, $^3J_{\text{HH}} = 6.9$ Hz, CH_3 DiPPE), 1.51 (dd, 6H, $^3J_{\text{HP}} = 15.5$ Hz, $^3J_{\text{HH}} = 7.5$ Hz, CH_3 DiPPE), 1.59 (dd, 2H, $^3J_{\text{HP}} = 3.0$, 8.0 Hz, Ni- CH_2), 1.65 (m, 2H, CH_2 DiPPE), 1.84 (m, 4H, CH_2 , CH DiPPE), 2.39 (sp, 2H, $^3J_{\text{HH}} = 7.0$ Hz, CH DiPPE), 6.93 (t, 1H, $^3J_{\text{HH}} = 7.4$ Hz, $p\text{-CH}_{\text{ar}}$ Ph), 6.99 (t, 2H, $^3J_{\text{HH}} = 7.4$ Hz, $m\text{-CH}_{\text{ar}}$ Ph), 7.12 (t, 2H, $^3J_{\text{HH}} = 6.3$ Hz, 3-CH_{ar} py), 7.56 (t, 1H, $^3J_{\text{HH}} = 7.2$ Hz, 4-CH_{ar} py), 8.0 (d, 2H, $^3J_{\text{HH}} = 5.7$ Hz, $o\text{-CH}_{\text{ar}}$ Ph), 8.41 (d, 2H, $^3J_{\text{HH}} = 5.0$ Hz, 2-CH_{ar} py). $^{31}\text{P}\{^1\text{H}\}$ (162 MHz, CD_2Cl_2 , 25 °C) δ 59.2, 72.4 (s). Data for **8a**: δ 1.0–1.3 (overlapping signals, 12H, CH_3 DiPPE); 1.7–1.4 (overlapping signals, 8H, 2 CH_2 + CH DiPPE), 2.31 (sp, 2H, $^3J_{\text{HH}} = 7.0$ Hz, CH DiPPE), 6.82 (t, 1H, $^3J_{\text{HH}} = 7.4$ Hz, $p\text{-CH}_{\text{ar}}$ Ph), 6.91 (t, 2H, $^3J_{\text{HH}} = 7.4$ Hz, $m\text{-CH}_{\text{ar}}$ Ph), 7.4–7.6 (overlapping multiplets, 4H, 3-CH_{ar} py and $o\text{-CH}$ Ph); 7.72 (t, 1H, $^3J_{\text{HH}} = 7.2$ Hz, 4-CH_{ar} py), 8.75 (d, 2H, $^3J_{\text{HH}} = 5.0$ Hz, 2-CH_{ar} py). $^{31}\text{P}\{^1\text{H}\}$ (162 MHz, CD_2Cl_2 , 25 °C): AX spin system: $\delta_{\text{A}} = 65.1$, $\delta_{\text{X}} = 72.1$, $^2J_{\text{AX}} = 11.4$ Hz.

$[\text{Ni}(\text{CH}_2\text{CMe}_2\text{Ph})(\text{DMAP})\text{DiPPE}][\text{TfO}]$, **9a**. To a solution of complex **4a** (110 mg, 0.24 mmol) in 20 mL of Et_2O , cooled to -70 °C, pyridinium triflate (55.6 mg, 0.24 mmol) was added, suspended in 25 mL of Et_2O . The mixture was stirred for 15 min at this temperature and then held for 30 min at -20 °C. Then, DMAP (30 mg, 0.24 mmol) was added, and the resulting suspension was stirred at room temperature for two hours. The suspension was filtered, and the yellow solid residue was washed with Et_2O (2×10 mL) and dried under vacuum. (Yield: 88%.) ^1H (400 MHz, $(\text{CD}_3)_2\text{CO}$, 25 °C): δ 0.99 (dd, 6H, $^3J_{\text{HP}} = 15.0$ Hz, $^3J_{\text{HH}} = 7.3$ Hz, CH_3 DiPPE), 1.12 (dd, 6H, $^3J_{\text{HP}} = 13.0$ Hz, $^3J_{\text{HH}} = 7.0$ Hz, CH_3 DiPPE), 1.28 (s, 6H, CMe_2), 1.36 (dd, 6H, $^3J_{\text{HP}} = 13.4$ Hz, $^3J_{\text{HH}} = 7.0$ Hz, CH_3 DiPPE), 1.49 (dd, 6H, $^3J_{\text{HP}} = 15.5$ Hz, $^3J_{\text{HH}} = 7.3$ Hz, CH_3 DiPPE), 1.58 (dd, 2H, $^3J_{\text{HP}} = 3.8$, 9.0 Hz, Ni- CH_2), 1.75 (m, 2H, CH_2 DiPPE), 2.0 (m, 4H, CH_2 , CH DiPPE), 2.42 (m, 2H, CH DiPPE), 3.0 (s, 6H, NMe_2 DMAP), 6.45 (d, 2H, $^3J_{\text{HH}} = 7.3$ Hz, DMAP), 6.91 (t, 1H, $^3J_{\text{HH}} = 7.3$ Hz, $p\text{-CH}_{\text{ar}}$ Ph), 7.01 (t, 2H, $^3J_{\text{HH}} = 8.0$ Hz, $m\text{-CH}_{\text{ar}}$ Ph), 7.17 (d, 2H, $^3J_{\text{HH}} = 7.2$ Hz, $o\text{-CH}_{\text{ar}}$ Ph), 8.07 (d, 2H, $^3J_{\text{HH}} = 7.5$ Hz, DMAP). $^{13}\text{C}\{^1\text{H}\}$ (100.6 MHz, $(\text{CD}_3)_2\text{CO}$, 25 °C): δ 18.4 (s, 2C, CH_3 DiPPE), 18.5 (m, 1C, CH_2 DiPPE), 18.7 (d, 2C, $^2J_{\text{CP}} = 2.0$ Hz, CH_3 DiPPE), 19.1 (d, 2C, $^2J_{\text{CP}} = 5.0$ Hz, CH_3 DiPPE), 20.8 (d, 2C, $^2J_{\text{CP}} = 2.0$ Hz, CH_3 DiPPE), 23.1 (dd, $^2J_{\text{CP}} = 20.0$, 26.0 Hz, Ni- CH_2), 24.7 (d, 2C, $^1J_{\text{CP}} = 15.0$ Hz, CH DiPPE), 26.1 (d, 2C, $^1J_{\text{CP}} = 26.0$ Hz, CH DiPPE), 34.3 (d, $^4J_{\text{CP}} = 5.0$ Hz, CMe_2), 39.1 (s, 2C, NMe_2 DMAP), 41.6 (s, CMe_2), 108.9 (s, 2C, $\text{C}_{\text{ar}}\text{H}$, DMAP), 125.0 (s, 1C, $p\text{-C}_{\text{ar}}\text{H}$ Ph), 126.3 (s, 2C, $\text{C}_{\text{ar}}\text{H}$ Ph), 128.4 (s, 2C, $\text{C}_{\text{ar}}\text{H}$ Ph), 150.3 (s, 2C, $\text{C}_{\text{ar}}\text{H}$, DMAP), 154.0 (s, 1C, C_{ar} , DMAP), 155.4 (s, 1C, $i\text{-C}_{\text{ar}}$ Ph). $^{31}\text{P}\{^1\text{H}\}$ (162 MHz, $(\text{CD}_3)_2\text{CO}$, 25 °C): δ 60.6, 73.0 (s).

$[\text{Ni}(\text{Me})(\text{py})(\text{DiPPE})][\text{TfO}]$, **10a**. A solution containing 100 mg (0.28 mmol) of the dimethyl precursor $[\text{NiMe}_2(\text{DiPPE})]$ in 20 mL of Et_2O and cooled to -65 °C was treated with a suspension of pyridinium triflate (44 mg, 0.28 mmol) in 20 mL of Et_2O . The mixture was stirred for 15 min at this temperature and then held for 4 h at 0 °C. A yellow solid was formed. The suspension was filtered, and the solid was washed with Et_2O (2×10 mL) and dried under vacuum. (Yield: 92%.) ^1H (400 MHz, CD_2Cl_2 , 25 °C): δ -0.07 (dd, 6H, $^3J_{\text{HP}} = 5.0$ Hz, Ni- CH_3), 0.98 (dd, 6H, $^3J_{\text{HP}} = 15.2$ Hz, $^3J_{\text{HH}} = 7.2$ Hz, CH_3 DiPPE), 1.19 (dd, 6H, $^3J_{\text{HP}} = 13.4$ Hz, $^3J_{\text{HH}} = 6.9$ Hz, CH_3 DiPPE), 1.34 (dd, 6H, $^3J_{\text{HP}} = 14.2$ Hz, $^3J_{\text{HH}} = 7.1$ Hz, CH_3 DiPPE), 1.40 (dd, 6H, $^3J_{\text{HP}} = 16.5$ Hz, $^3J_{\text{HH}} = 7.2$ Hz, CH_3 DiPPE), 1.71 (m, 2H, CH_2 DiPPE), 1.91 (m, 2H, CH_2 DiPPE), 2.01 (m, 2H, CH DiPPE), 2.33 (m, 2H, CH DiPPE), 7.59

(t, 2H, $^3J_{\text{HH}} = 6.6$ Hz, 3- CH_{ar} py), 7.91 (t, 1H, $^3J_{\text{HH}} = 7.3$ Hz, 4- CH_{ar} py), 8.71 (d, 2H, $^3J_{\text{HH}} = 4.4$ Hz, 2- CH_{ar} py). $^{13}\text{C}\{^1\text{H}\}$ (100.6 MHz, CD_2Cl_2 , 25 °C): δ 4.2 (dd, 1C, $^2J_{\text{CP}} = 35.0$, 59.0 Hz, Ni- CH_3), 17.8 (dd, 1C, $^1J_{\text{CP}} = 24.0$ Hz, $^2J_{\text{CP}} = 10.0$ Hz, CH_2 DiPPE), 18.5 (s, 2C, CH_3 DiPPE), 18.8 (s, 2C, CH_3 DiPPE), 19.1 (s, 2C, CH_3 DiPPE), 20.5 (s, 2C, CH_3 DiPPE), 23.3 (dd, 1C, $^1J_{\text{CP}} = 23.0$ Hz, $^2J_{\text{CP}} = 20.0$ Hz, CH_2 DiPPE), 24.1 (d, 2C, $^1J_{\text{CP}} = 17.0$ Hz, CH DiPPE), 26.3 (d, 2C, $^1J_{\text{CP}} = 29.0$ Hz, CH DiPPE), 126.7 (s, 2C, C_{arH} py), 138.6 (s, 1C, C_{arH} py), 150.1 (s, 2C, C_{arH} py). $^{31}\text{P}\{^1\text{H}\}$ (162 MHz, CD_2Cl_2 , 25 °C): δ 64.3, 81.6 (d, $^2J_{\text{PP}} = 4.8$ Hz).

[Ni(Me)(DMAP)(DiPPE)][TfO] **11a**. A sample of 110 mg (0.31 mmol) of the dimethyl precursor $[\text{NiMe}_2(\text{DiPPE})]$ was dissolved in 20 mL of Et_2O , the solution was cooled to -70 °C, and a suspension of 70 mg (0.31 mmol) of pyridinium triflate in 20 mL of Et_2O was added. The mixture was stirred for 15 min at this temperature and then held for one hour at 0 °C, and a solution of 38 mg (0.31 mmol) de DMAP in 10 mL of Et_2O was added. The resulting suspension was stirred at room temperature for four hours, filtered, and the yellow residue washed with Et_2O (2×10 mL) and dissolved in a mixture of acetone/hexane. After cooling the solution to -30 °C overnight, compound **11a** was isolated as yellow crystals. (Yield: 87%.) Anal. Calcd. for $\text{C}_{23}\text{H}_{45}\text{F}_3\text{N}_2\text{NiO}_3\text{P}_2\text{S}$: C, 45.49; H, 7.47. Found: C, 44.64; H, 6.64. ^1H (400 MHz, $(\text{CD}_3)_2\text{CO}$, 25 °C): δ -0.14 (dd, 3H, $^3J_{\text{HP}} = 4.0$, 5.3 Hz, Ni- CH_3), 1.07 (dd, 6H, $^3J_{\text{HP}} = 15.0$ Hz, $^3J_{\text{HH}} = 7.3$ Hz, CH_3 DiPPE), 1.23 (dd, 6H, $^3J_{\text{HP}} = 13.3$ Hz, $^3J_{\text{HH}} = 7.0$ Hz, CH_3 DiPPE), 1.34 (dd, 6H, $^3J_{\text{HP}} = 14.0$ Hz, $^3J_{\text{HH}} = 7.0$ Hz, CH_3 DiPPE), 1.39 (dd, 6H, $^3J_{\text{HP}} = 16.2$ Hz, $^3J_{\text{HH}} = 7.3$ Hz, CH_3 DiPPE), 1.80 (m, 2H, CH_2 DiPPE), 2.0 (m, 4H, CH_2 , CH DiPPE), 2.40 (m, 2H, CH DiPPE), 3.1 (s, 6H, NMe_2 DMAP), 6.85 (d, 2H, $^3J_{\text{HH}} = 7.0$ Hz, CH_{ar} DMAP), 8.30 (d, 2H, $^3J_{\text{HH}} = 6.1$ Hz, CH_{ar} DMAP). $^{13}\text{C}\{^1\text{H}\}$ (100.6 MHz, $(\text{CD}_3)_2\text{CO}$, 25 °C): δ 3.3 (dd, 1C, $^2J_{\text{CP}} = 35.0$, 63.0 Hz, Ni- CH_3), 18.0 (dd, 1C, $^1J_{\text{CP}} = 24.0$ Hz, $^2J_{\text{CP}} = 10.0$ Hz, CH_2 DiPPE), 18.6 (s, 2C, CH_3 DiPPE), 18.9 (s, 2C, CH_3 DiPPE), 19.2 (d, 2C, $^2J_{\text{CP}} = 4.0$ Hz, CH_3 DiPPE), 20.5 (s, 2C, CH_3 DiPPE), 23.6 (dd, 1C, $^1J_{\text{CP}} = 24.0$ Hz, $^2J_{\text{CP}} = 20.0$ Hz, CH_2 DiPPE), 24.5 (d, 2C, $^1J_{\text{CP}} = 17.0$ Hz, CH DiPPE), 26.4 (d, 2C, $^1J_{\text{CP}} = 29.0$ Hz, CH DiPPE), 39.2 (s, 2C Me DMAP), 109.4 (s, 2C, C_{arH} DMAP), 149.7 (s, 2C, C_{arH} DMAP), 155.4 (s, 1C, C_{ar} DMAP). $^{31}\text{P}\{^1\text{H}\}$ (162 MHz, $(\text{CD}_3)_2\text{CO}$, 25 °C): δ 65.3, 81.7 (d, $^2J_{\text{PP}} = 5.0$ Hz).

Synthesis of [Ni(Me)(DMAP)(DiPPP)][TfO], **11b**. To a solution of 130 mg (0.31 mmol) of complex **53b** in 20 mL of Et_2O cooled to -70 °C, pyridinium triflate (73 mg, 0.31 mmol) suspended in 20 mL of Et_2O was added. The mixture was stirred at this temperature for 15 min and then held for two hours at -20 °C, and a solution of 39 mg (0.31 mmol) of DMAP dissolved in 10 mL of Et_2O was added. The resulting suspension was stirred at room temperature for two hours, filtered, and the yellow residue washed with Et_2O (2×10 mL) and dried under vacuum. (Yield: 87%.) ^1H (400 MHz, $(\text{CD}_3)_2\text{CO}$, 25 °C): δ -0.18 (pt, 3H, $^3J_{\text{HP}} = 4.3$ Hz, Ni- CH_3), 1.20 (dd, 12H, CH_3 DiPPP), 1.33 (dd, 6H, $^3J_{\text{HP}} = 13.0$ Hz, $^3J_{\text{HH}} = 6.9$ Hz, CH_3 DiPPP), 1.43 (m, 2H, CH_2 DiPPP), 1.54 (dd, 6H, $^3J_{\text{HP}} = 17.0$ Hz, $^3J_{\text{HH}} = 7.4$ Hz, CH_3 DiPPP), 1.63 (m, 2H, CH_2 DiPPP), 1.93 (m, 4H, CH_2 , CH DiPPP), 2.31 (m, 2H CH DiPPP), 3.10 (s, 6H, NMe_2 DMAP), 6.85 (d, 2H, $^3J_{\text{HH}} = 5.9$ Hz, CH_{ar} DMAP), 8.34 (d, 2H, $^3J_{\text{HH}} = 5.9$ Hz, CH_{ar} DMAP). $^{13}\text{C}\{^1\text{H}\}$ (100.6 MHz, $(\text{CD}_3)_2\text{CO}$, 25 °C): δ 5.9 (dd, 1C, $^2J_{\text{CP}} = 38.0$, 59.0 Hz, Ni- CH_3), 17.5 (dd, 1C, $^1J_{\text{CP}} = 18.0$ Hz, $^2J_{\text{CP}} = 10.0$ Hz, CH_2 DiPPP), 18.0 (s, 2C, CH_3 DiPPP), 18.7 (t, 1C, $^1J_{\text{CP}} = 18.0$ Hz, CH_2 DiPPP), 18.9 (s, 2C, CH_3 DiPPP), 19.7 (s, 2C, CH_3 DiPPP), 21.7 (t, 1C, $^1J_{\text{CP}} = 18.0$ Hz, CH_2 DiPPP), 22.3 (s, 2C, CH_3 DiPPP), 25.3 (t, 1C, $^1J_{\text{CP}} = 18.0$ Hz, CH DiPPP), 27.4 (t, 1C, $^1J_{\text{CP}} = 31.0$ Hz, CH_2 DiPPP), 39.2 (s, 2C Me DMAP), 109.5 (s, 2C, C_{arH} DMAP), 149.9 (s, 2C, C_{arH} DMAP), 155.4 (s, 1C, C_{ar} DMAP). $^{31}\text{P}\{^1\text{H}\}$ (162 MHz, $(\text{CD}_3)_2\text{CO}$, 25 °C): δ 7.1, 34.8 (d, $^2J_{\text{PP}} = 37.0$ Hz).

[Ni(Ph)(PMe₃)DiPPE][BAR'₄], **12**. A solution of complex **58a** (113 mg, 0.25 mmol) in 30 mL of Et_2O cooled to -70 °C was treated with 232 mg (0.25 mmol) of $[\text{HPMe}_3][\text{BAR}'_4]$, and the resulting mixture was allowed to reach room temperature and stirred at this temperature for three hours. The mixture was evaporated to dryness, and the residue was extracted with 20 mL of Et_2O . The solution was filtered, and some hexane was added. Compound **12** was isolated as yellow crystals after cooling the solution to -30 °C overnight. (Yield: 86%.) Anal. Calcd. for $\text{C}_{55}\text{H}_{58}\text{B F}_{24}\text{NiP}_3$: C, 49.39; H, 4.37. Found: C, 49.35; H, 3.98.

^1H (400 MHz, CD_2Cl_2 , 25 °C): δ 0.97 (dd, 6H, $^3J_{\text{HP}} = 15.8$ Hz, $^3J_{\text{HH}} = 7.7$ Hz, CH_3 DiPPE), 1.08 (dd, 6H, $^3J_{\text{HP}} = 12.9$ Hz, $^3J_{\text{HH}} = 7.2$ Hz, CH_3 DiPPE), 1.14 (d, 9H, $^2J_{\text{HP}} = 8.0$ Hz, PMe_3), 1.30 (dd, 6H, $^3J_{\text{HP}} = 14.0$ Hz, $^3J_{\text{HH}} = 6.6$ Hz, CH_3 DiPPE), 1.34 (dd, 6H, $^3J_{\text{HP}} = 17.5$ Hz, $^3J_{\text{HH}} = 6.7$ Hz, CH_3 DiPPE), 1.88 (m, 4H, CH_2 DiPPE), 2.17 (m, 4H, CH DiPPE), 6.99 (t, 1H, $^3J_{\text{HH}} = 6.6$ Hz, $p\text{-CH}_{\text{ar}}$ Ph), 7.14 (t, 2H, $^3J_{\text{HH}} = 7.1$ Hz, $m\text{-CH}_{\text{ar}}$ Ph), 7.27 (m, 2H, $o\text{-CH}_{\text{ar}}$ Ph), 7.61 (s, 4H, CH_{ar} BAR'_4), 7.77 (s, 8H, CH_{ar} BAR'_4). $^{13}\text{C}\{^1\text{H}\}$ (100.6 MHz, CD_2Cl_2 , 25 °C): δ 15.3 (d, 3C, $^1J_{\text{CP}} = 30$ Hz, PMe_3), 17.5 (s, 2C, CH_3 DiPPE), 18.8 (d, 2C, $^2J_{\text{CP}} = 3.0$ Hz, CH_3 DiPPE), 19.1 (m, 1C, CH_2 DiPPE), 19.5 (s, 2C, CH_3 DiPPE), 21.3 (pt, 1C, $^*J_{\text{CP}} = 18$ Hz, CH_2 DiPPE), 21.6 (d, 2C, $^2J_{\text{CP}} = 6.0$ Hz, CH_3 DiPPE), 25.0 (d, 2C, $^1J_{\text{CP}} = 26$ Hz, CH DiPPE), 26.5 (d, 2C, $^1J_{\text{CP}} = 19$ Hz, CH DiPPE), 117.8 (s, 4C, $\text{C}_{\text{ar}}\text{H}$ BAR'_4), 124.4 (s, 1C, $\text{C}_{\text{ar}}\text{H}$ Ph), 124.9 (c, 8C, $^1J_{\text{CF}} = 272$ Hz, CF_3 BAR'_4), 128.2 (s, 2C, $\text{C}_{\text{ar}}\text{H}$ Ph), 129.2 (c, 8C, $^2J_{\text{CF}} = 32$ Hz, $\text{C}_{\text{ar}}\text{CF}_3$ BAR'_4), 135.1 (s, 8C, $\text{C}_{\text{ar}}\text{H}$ BAR'_4), 137.0 (s, 2C, $\text{C}_{\text{ar}}\text{H}$ Ph), 150.0 (m, 1C, C_{ar} Ph), 162.1 (c, 4C, $^1J_{\text{CB}} = 46$ Hz, CB BAR'_4). $^{31}\text{P}\{^1\text{H}\}$ (162 MHz, CD_2Cl_2 , 25 °C): δ 18.8 (dd, $^2J_{\text{PP}} = 30$, 243 Hz), 68.9 (dd, $^2J_{\text{PP}} = 18$, 243 Hz), 76.5 (dd, $^2J_{\text{PP}} = 18$, 29 Hz).

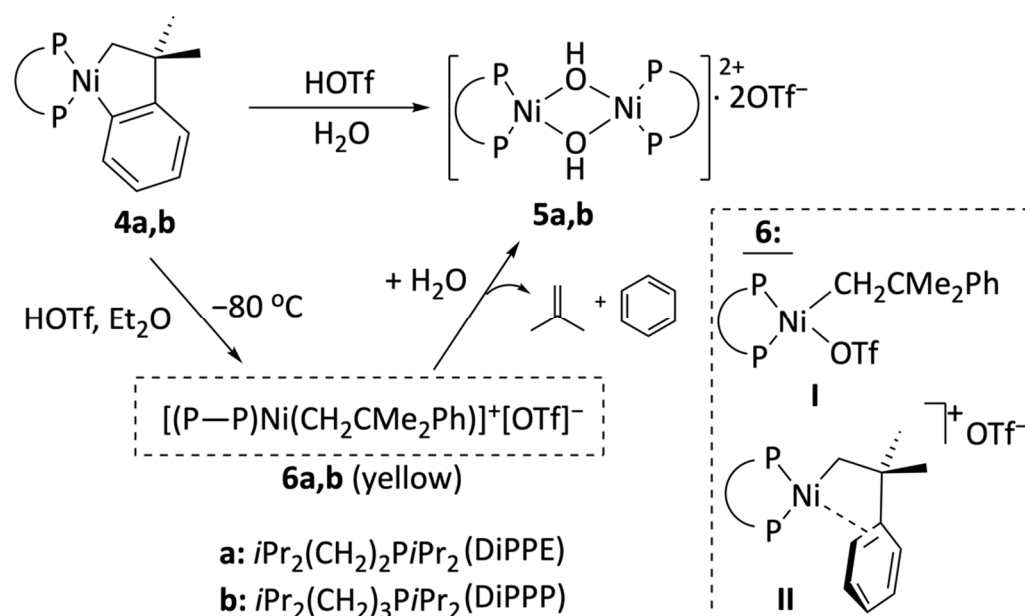
3. Computational Details

All calculations were made with the commercial software Spartan'20 [44]. Starting points for the optimization search were located using the robust PBE/6–31G* method. Geometry optimizations were made using m–GGA functional M06–L functional, the def2–SVPD basis functions, and the CPCM implicit model solvent available in Spartan, using the DICHLOROMETHANE option ($\epsilon = 8.93$). The energy gradient convergence criterium was tightened from Spartan's default value 3×10^{-4} to 5×10^{-5} erg-bohr $^{-1}$. Electronic (SCF) energies were refined with a single point calculation at the M06/def2–TZVPPD level, with the SCF convergence criterion set to "HIGH". All stationary points were checked to have zero (stable intermediates) or one imaginary frequency (transition states). Single-point calculations were accelerated using the "dual basis" option, which specifies that SCF convergence is achieved at the def2–TZVP level and then corrected perturbatively for the effect of additional diffuse and polarization functions. Thermal corrections (TC) were computed at 298.15 (25 °C) and 1 atmosphere. To calculate the solvent correction (SC), we performed an inexpensive additional gas phase single-point energy calculation on optimized geometries at the M06–L/def2–SVPD level (i.e., omitting the solvent calculation), therefore, $\text{SC} = \text{E}(\text{SCF}, \text{CPCM}) - \text{E}(\text{SCF}, \text{gas phase})$, at the M06–L/def2–SVPD level. In addition to reducing the computational cost, this procedure has the advantage of computing the solvent effect at a level of the theory similar to that used for the parametrization of the CPCM model. The refined G° values were calculated for each molecule as $G^\circ = \text{E}(\text{SCF}, \text{M06/def2–TZVPPD}) + \text{TC} + \text{SC}$. ZPE-corrected SCF energy data also refer to single-point M06/def2–TZVPPD calculations and include the solvent correction, i.e., $\text{E}_{(\text{SCF} + \text{ZPE})} = \text{E}(\text{SCF} + \text{SC} + \text{ZPE})$. When the transition states closely resemble that of the highest-energy ground state (e.g., Ni–TS1), the free energy composed by this approximate summation procedure may be slightly below that of this ground state. To avoid this artifact, the free energy of the transition state was computed by adding the difference calculated at the geometry optimization level to that of the highest-lying ground state. Free-energy profiles were generated using the freely available online tool EverPlot [45].

4. Results and Discussion

Reactions of nickelacyclic complexes 4a,b with acidic derivatives of low-coordination capacity anions. Anticipating the high reactivity and lower kinetic stability of nickel complexes, in this work, we have decided to focus our study on the bulky diphosphine 1,2–bis(diisopropylphosphino)ethane (DiPPE) instead of the less-demanding ligand DMPE, previously used with palladium. In addition, we conducted some experiments with the related ligand 1,3–bis(diisopropylphosphino)propane (DiPPP), which differs only in having one additional methylene group in its backbone. To this end, we used the previously reported [43] nickelacycles 4a and 4b.

Adding one equivalent of triflic acid to cold solutions of either of these metallacycles in diethyl ether leads to yellow suspensions that, on stirring at room temperature for ca. one hour, change to a reddish-orange color. The products were easily isolated in high yields and characterized based on their IR, NMR, and analytical data. These were identified as the binuclear hydroxo-bridged dimeric complexes with the composition $[\{\text{Ni}(\mu\text{-OH})(\text{P-P})\}_2]^{2+}[\text{OTf}^-]_2$, **5a** and **5b** ($\text{P-P} = \text{DiPPE}$ or DiPPP , see Scheme 3). Their ^1H spectra show a high-field resonance (**5a**, -1.51 ppm; **5b**, -3.27 ppm) for the hydroxyl protons, but no additional signals other than those of the diphosphine ligands were observed in the proton or ^{13}C NMR spectra, consistent with the loss of the hydrocarbyl ligand. In anhydrous CD_2Cl_2 , the characteristic OH signal of **5a** is split in a quintet with $J_{\text{HP}} \approx 2$ Hz by coupling with four chemically equivalent ^{31}P nuclei. Although the H-P coupling was not resolved in the case of **5b**, both complexes exhibit simple $^{31}\text{P}\{^1\text{H}\}$ spectra consisting of a single sharp singlet, as expected for their highly symmetrical structures. The characteristic IR absorption bands for the **5a** and **5b** O-H stretches were observed at 3954 and 3513 cm^{-1} , respectively. In addition, the spectral data for **5a** are entirely consistent with those reported by J. García and colleagues, who resolved the crystal structure of this compound [46].



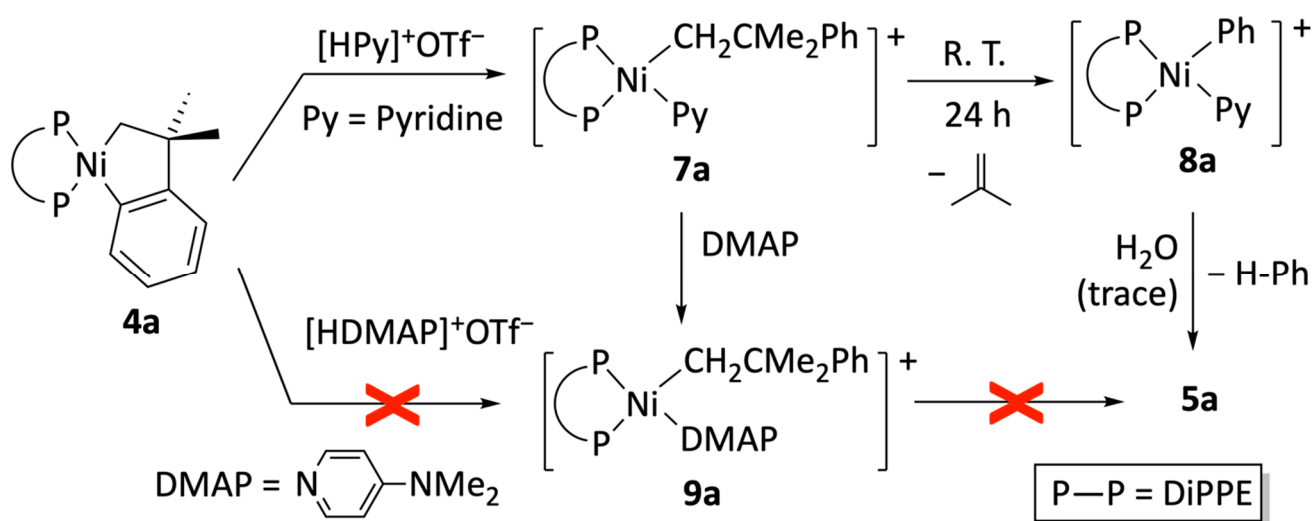
Scheme 3. Reaction of complexes **4a** and **4b** with triflic acid.

It has been shown that electrophiles, including conventional Brønsted acids, react selectively with nickel or palladium benzometallacyclopentenes of type **4**, cleaving the M-aryl bond to yield neophyl derivatives [37,47–49]. The course of the reactions of **4a** and **4b** with triflic acid also fit this trend. However, the initially formed products are unstable, reacting with trace amounts of water to yield the corresponding hydroxides. Accordingly, if the initial yellow precipitate formed from **4a** and HOTf is filtered off from the solution, and its ^1H and $^{31}\text{P}\{^1\text{H}\}$ NMR spectra are quickly recorded, these show the typical features expected for a non-symmetrical neophylnickel-triflate species, **6**. Thus, the $^{31}\text{P}\{^1\text{H}\}$ spectrum of **6a** displays two doublets (at 57 and 69 ppm; $^2J_{\text{PP}} = 9$ Hz), and all signals for the nickel-bound neophyl group were identified in the ^1H spectrum. As expected, the signal for the nickel-bound CH_2 , observed in the high field region (0.78 ppm), is split into a doublet of doublets by coupling with two chemically inequivalent ^{31}P nuclei (14.0 and 4.8 Hz). Similar observations were made for **6b** (see the experimental part). The NMR data alone cannot unambiguously tell the exact coordination mode of the neophyl ligand in these complexes. However, no additional signals for coordinated solvent or water were observed in the ^1H spectra of **6a** or **6b**. As depicted in Scheme 3, complexes

6 could exist as either a neutral species with a sigma ligand (I) or as a cationic species, with an intramolecular π -arene interaction, similar to the Pd complex **1** (II). The chemical shift of the ^1H NMR Ni-CH₂ signal of **6a** is unusually upfield-shifted compared to nickel complexes with terminally coordinated neophyl derivatives or the starting metallacycles **4a** or **4b** (ca. 1.5–2.0 ppm) [43,50]. A similar shielding of the methylene signals is observed in the ^1H NMR spectra of known Pd(II) σ,π -neophyl derivatives, such as **1** [37,39,48]. This suggests that **5a** (and possibly **5b**) might have an ionic structure of type II. Moreover, a close analog of **6** with a σ,π -neophylnickel cation but supported by the even bulkier diphosphine DtBPE (1,2-(di-*t*-butylphosphino)ethane) was synthesized and structurally characterized by Hillhouse [51]. Interestingly, this complex was crystallized in the presence of donor solvents THF and Et₂O, yet it has a type II structure. Its Ni-C(*ipso*) bond, 2.478(4) Å, is quite long, even for a π -bond, which suggests that the arene interaction is weak, probably due to steric repulsions with the DtBPE ligand. Unfortunately, the methylene resonance was not located due to extensive signal overlapping in the ^1H aliphatic region, preventing a comparison with **6a**.

Complexes **6a** and **b** are thermally unstable in CD₂Cl₂. The transformation of **6a** into the hydroxide **5a** is complete within a few hours at room temperature, even if our NMR solvent is routinely dried by refluxing over CaH₂ (see the experimental part). The decomposition was accompanied by the formation of an equimolar amount of isobutene (signals at 1.74 and 4.66 ppm, intensity ratio 3:1) and benzene (7.34 ppm). No *t*-butylbenzene, the signature of a hypothetical Ni-CH₂ hydrolysis, was detected. The *t*-Bu of *t*-butylbenzene would give a conspicuous singlet at ca. 1.31 ppm, next to the CMe₂ resonance of **6a**, at 1.40 ppm. These data conclusively demonstrate that the decay of complexes **6** does not involve direct hydrolysis but quantitative β -Ph elimination. Consequently, the hydroxides **5** are formed from the unstable phenyl species arising from it.

To confirm the β -Ph elimination mechanism, we decided to explore the protonation of **4a** with the conjugate acids of bases of different coordination strengths that, once deprotonated, could bind to the products. The base-stabilized neophyl intermediates might be stable enough to allow detection or isolation. In the first attempt, we reacted pyridinium triflate with **4a** (Scheme 4). The neophyl-pyridine adduct, **7a**, also precipitates when the diethyl ether reaction is conducted at -60 °C. The yellow precipitate was collected, and its ^1H and $^{31}\text{P}\{^1\text{H}\}$ NMR spectra were recorded in a CD₂Cl₂ solution at room temperature. Although the pyridine ligand enhances its thermal stability, **7a** still decays via β -Ph elimination over 24 h, as indicated by the formation of isobutene and the phenyl complex **8a** (see Figure 1). Complex **8a** was identified based on its ^1H and $^{31}\text{P}\{^1\text{H}\}$ NMR spectra, but it could not be isolated pure, as it is prone to hydrolysis and is always contaminated with some hydroxide (**5a**).



Scheme 4. Reactions of **4a** with pyridinium and 4-dimethylaminopyridinium triflate. The cationic complex **9a** is not formed directly from **4a**, but it could be synthesized by a ligand exchange reaction from **7a**.

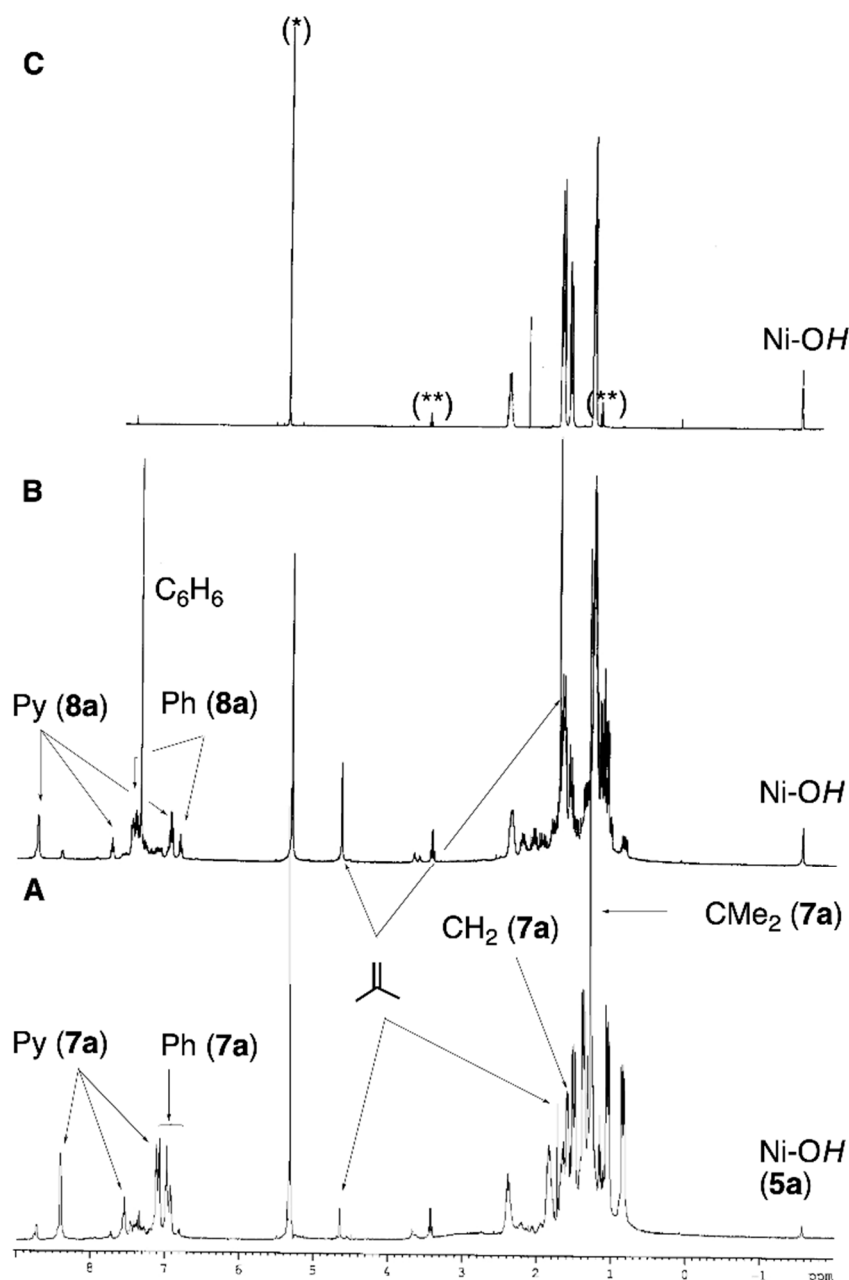
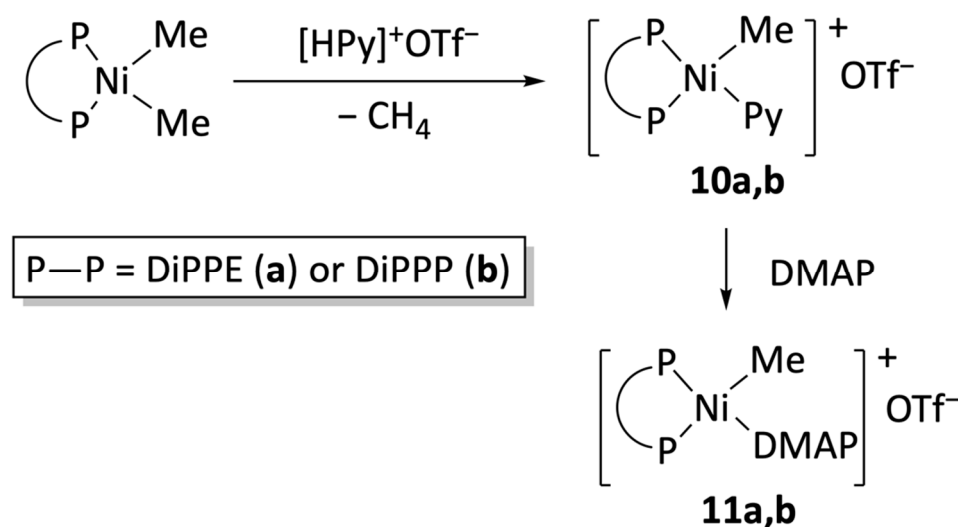


Figure 1. Evolution of a ^1H NMR spectra of a solution of **7a** in CD_2Cl_2 (residual peak for the solvent and traces of diethyl ether are marked (*) and (**), respectively). (A) A freshly prepared solution from the yellow precipitate formed in the reaction of **4a** with one equivalent of pyridinium triflate. Small amounts of **8a** and hydroxide **5a** are already noticeable. (B) The same sample, after 24 h at room temperature. The main species is already **8a**, along with isobutene, benzene, and a more significant amount of **5a**. (C) A spectrum of a purified sample of **5a** for reference.

To generate more stable neophyl complexes amenable to complete spectroscopic characterization, we considered replacing pyridine with *p*-dimethylamino pyridine, a qualitatively similar but stronger electron-donor ligand. Remarkably, *p*-dimethylamino-pyridinium triflate proved to be an acid too weak to cleave a Ni–C(aryl) bond of metal-cycles **4**. Therefore, as shown in Scheme 4, we first generated complex **7a**, and then the pyridine ligand was exchanged in situ with one equivalent of DMAP. In this way, analytically pure **9a** was obtained, with an excellent yield. The latter proved stable in solution and has been fully characterized by the usual ensemble of multinuclear NMR, IR,

and elemental analyses. The spectroscopic features of **9a** are very similar to those of the thermally sensitive **7a** and confirmed the previous assignments based on solution ^1H and ^{31}P data only. On the other hand, we have performed preliminary research in the DiPPP system, which confirmed that the same route could be applied to prepare derivatives **7b** and **9b**. Selected data for the latter two compounds are provided in the Materials and Methods Section.

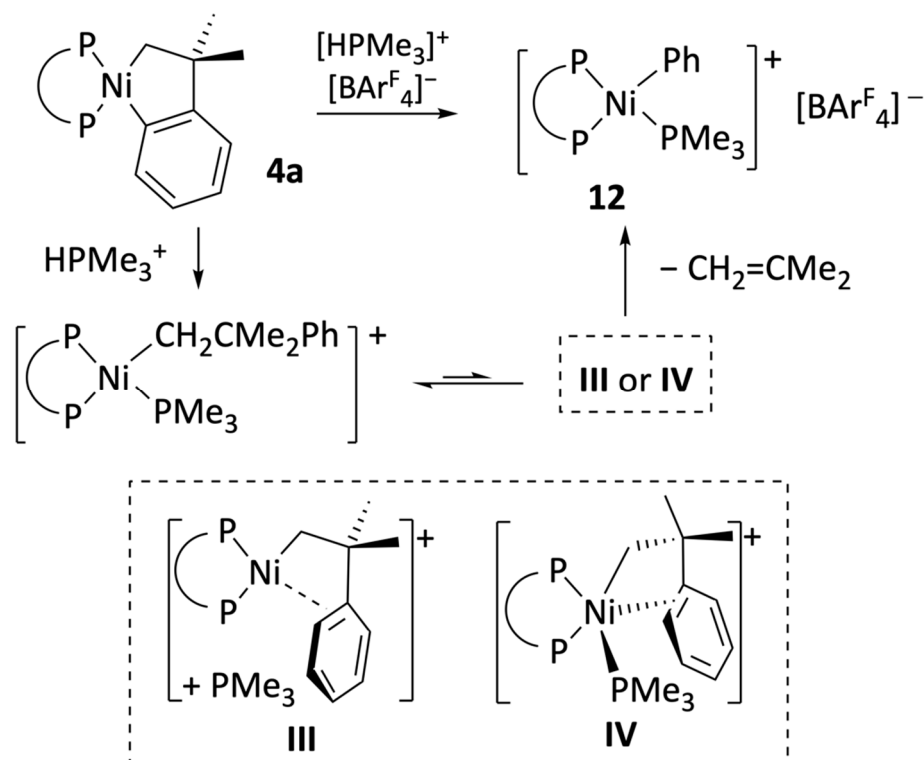
Cationic organonickel complexes, such as **8**, containing diphosphine and pyridine ligands are rare. To our knowledge, only a couple of aryl derivatives of composition $[\text{Ni}(\text{Ar})(\gamma\text{-Pic})(\text{DPPE})]^+(\text{BF}_4)^-$ have been briefly mentioned in the literature ($\gamma\text{-Pic}$ = 4 methylpyridine, Ar = mesityl or 3,5-dichlorophenyl) [52,53]. However, the hydrolytic sensitivity of the pyridine-stabilized complex **8a** is quite surprising. To test whether this is a general property of organonickel derivatives with this configuration or if it is a specific property of this phenyl complex, we decided to synthesize methyl analogs of **8** by protonation of the known dimethyl complexes [43] $[\text{NiMe}_2(\text{P}-\text{P})]$ with pyridinium triflate (Scheme 5). The pyridine-containing methyl complexes **10** were isolated and fully characterized. For the sake of completeness, we also report similar data for the corresponding DMAP adducts (**11a,b**), which were used to help in the spectroscopic assignment of the NMR spectra of the less stable complexes (Scheme 5). All these methylnickel derivatives exhibit normal hydrolytic behavior. Solutions of **10** in dichloromethane can be stored for extended periods without noticeable formation of hydroxide **5a**, confirming the high reactivity of the Ni-aryl linkage in this type of cationic complexes. This issue is discussed in more depth in the computational section.



Scheme 5. Syntheses of stable cationic alkyl-nickel adducts of pyridine.

Following a similar approach, we have briefly investigated the reaction of complex **4a** with an acidic trimethylphosphonium salt. In this case, we used the crystalline derivative $[\text{HPMe}_3]^+[\text{BAR}'_4]^-$ ($\text{Ar}' = 3,5\text{-C}_6\text{H}_5(\text{CF}_3)_2$) for practical reasons. In view of the thermal stability of the DMAP complexes **9**, we expected that the interaction **4a** with one equivalent of the trimethylphosphonium salt would also yield a stable neophyl derivative, $[\text{Ni}(\text{CH}_2\text{CMe}_2\text{Ph})(\text{PMe}_3)(\text{DiPPE})]^+[\text{BAR}'_4]^-$. However, the standard workup of the reaction mixture led to the isolation of the phenyl derivative $[\text{Ni}(\text{Ph})(\text{PMe}_3)(\text{DiPPE})]^+[\text{BAR}'_4]^-$ (**12**) in high yield, which was readily identified based on its NMR spectra (Scheme 6). This result is surprising because, as mentioned in the introduction, the similar palladium complex $[\text{Pd}(\text{CH}_2\text{CMe}_2\text{Ph})(\text{PMe}_3)(\text{DMPE})]^+[\text{BAR}'_4]^-$ is indefinitely stable in solution and only decays in the presence of the π -arene complex $[\text{Pd}(\sigma,\pi\text{-CH}_2\text{CMe}_2\text{Ph})(\text{DMPE})]^+$ (**1**), which is the agent that spontaneously undergoes $\beta\text{-Ph}$ elimination [39]. The comparatively facile isobutene de-insertion from the nickel neophyl- PMe_3 intermediate poses an intriguing

mechanistic problem, as shown in Scheme 6. It could be that the nickel system does not require the intermediacy of the $[\text{Ni}(\sigma,\pi\text{-CH}_2\text{CMe}_2\text{Ph})(\text{DiPPE})]^+$ cation (**III**) but proceeds through the pentacoordinate intermediate, **IV**. The latter might directly experience the $\beta\text{-Ph}$ abstraction to afford complex **12** without PMe_3 dissociation. This mechanism implies the existence of the reverse process involving associative olefin insertion through the same transition state, which might have consequences for some nickel-catalyzed reactions, particularly the Mizoroki–Heck reaction. This possibility will also be addressed in the computational section.



Scheme 6. Two possible mechanisms for $\beta\text{-Ph}$ elimination in 16-electron neophylnickel complexes: dissociative, involving intermediate **III**, or direct, through the 18-electron intermediate **IV**.

Computational analyses of reaction mechanisms with nickel and palladium. To compare the relative tendencies of nickel and palladium compounds to undergo $\beta\text{-Ph}$ elimination, we chose to compute the energy barriers in the structurally simpler derivatives with DMPE for both palladium and nickel, even when the latter was not investigated. This approach has advantages not only for limiting the conformational cost of modeling the *i*-Pr substituents but also allows a more realistic comparison of both metals. We chose the M06 family of functionals to perform the analyses because these provide a good description of non-covalent dispersive forces and steric repulsions that likely play a major role in the bonding of $\pi\text{-arene}$ M(II) cations. The less demanding M06-L functional, with a double-z basis, was used for geometry optimization and then complemented with a single-point energy calculation at the M06/triple-zeta quality basis functions level of the theory for energy calculations. The solvent was modeled as dichloromethane through the whole optimization procedure. As a benchmark of the geometry performance of this method, we optimized the geometry of Ni and Pd $\sigma,\pi\text{-neophyl}$ complexes whose experimental X-ray data were available in the literature [39,51]. These are compared in Figure 2.

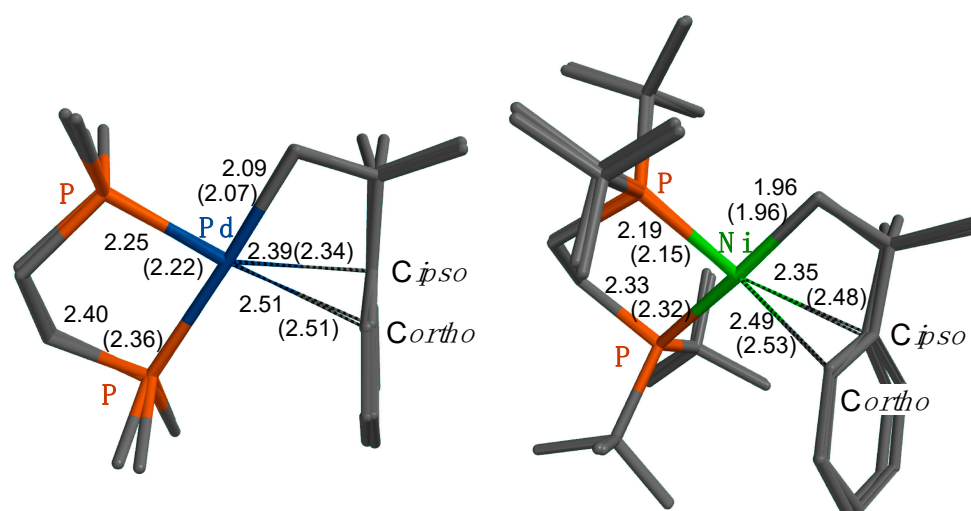
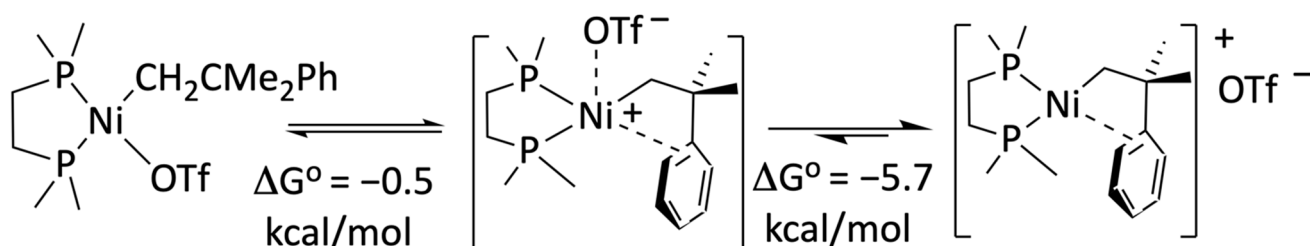


Figure 2. Superimposed geometries (tube models, hydrogen atoms have been omitted for clarity) showing selected distances (Å) computed at the M06-L/def2-SVPD level and X-ray diffraction data (in parentheses) for $[\text{Pd}(\text{CH}_2\text{CMe}_2\text{Ph})(\text{DMPE})]^+$ (**1**) [39] and $[\text{Ni}(\text{CH}_2\text{CMe}_2\text{Ph})(\text{DtBPE})]^+$ [51].

As can be seen, there is an excellent concordance between the calculation and the experimental X-ray diffraction data. The mean deviation of the reference values is less than 2% for both the Pd and Ni complexes. Not surprisingly, the most significant differences are found in the $\text{M}\cdots\text{C}(\text{ipso})$ distance, which reflects the delicate equilibrium between the weak attractive π -arene interaction and the steric interactions with the ligand and packing forces in the solid state. Perhaps for this reason, we found a significant improvement in the π -bond distances by adding diffuse functions (def2-SVPD) to the def2-SVP basis frequently used in geometry optimization. These repulsive forces are maximum for the nickel complex, which bears the bulky DtBPE ligand. The very long $\text{Ni}\cdots\text{C}(\text{ipso})$ bond predicted by the calculation (2.35 Å) is *even longer* in the crystal structure (2.48 Å). This suggests that, in this case, crystal packing forces may be distorting the weak π -Ni-arene interaction. For the sake of comparison, Figure S1 lists the π -bond distances computed for the Ni-DMPE (**6'**), DiPPE, and DtBPE σ,π -neophyl complexes, as well as those of the palladium model **1'** (see the SI for other molecular drawings; the apostrophe is used from now on to distinguish computational models from their experimental counterparts). As can be seen, as the steric bulk of the diphosphine increases, there is an elongation of the π Ni \cdots Ph interaction. This is strongest in **6'**, as revealed by shorter π Ni \cdots C(ipso) and Ni \cdots C(ortho) bonds, 2.18 and 2.30 Å, respectively. These distances are comparable to those in typical Ni(II)- π -arene interactions [54,55].

As mentioned before, our NMR data suggest that, at least in **6a**, the neophyl ligand likely coordinates in the σ,π -mode, as represented in **II**, rather than the triflate-alkyl structure of type **I** (see Scheme 3). To throw light on this issue, we have carefully examined both possible coordination models in the computational model (**6'**). Previously, we analyzed the different conformations of the neophyl ligand using a molecular mechanics approach with a frozen metal coordination unit. Then, the restrictions were removed, and the geometry of each of the conformers was re-optimized at the usual level of the DFT theory, including the solvent treatment. Seven local minima, four within 1 Kcal/mol on the potential energy surface (Figure S2 and Table S2 in the Supplementary Materials). Two of these (the absolute minimum, M001, and M003) have square-pyramidal geometries, where the basal plane greatly resembles **II**, and the triflate anion binds at the axial position with a rather Ni \cdots OTf, at ca. 2.3 Å. The rest exhibit more or less square-planar environments of type **I**, with in-plane Ni-OTf bond lengths of ca. 2.02–2.09 Å and the neophyl fragment adopting various configurations. Although we cannot predict the structure of complexes **6** in the solid state, M001 and M003 could be regarded as contact ion pairs of the π -arene

cation **6'** with the triflate anion. The entropy-driven complete dissociation of the triflate anion is granted by the significant exergonic balance, which amounts to -5.7 Kcal/mol relative stable of the pentacoordinate complexes, as represented in Scheme 7. Therefore, nickel complexes of type **6'** would most likely exist in dichloromethane solution as discrete π -arene stabilized ions. The same could be said of their real-world counterpart **6a**, in agreement with the above-discussed NMR hints.



Scheme 7. Free energy relationship of a neutral, square planar nickel triflate complex with a conventional σ -alkyl interaction, a pentacoordinated π -arene triflate complex, and fully dissociated ions.

For completeness, we repeated this treatment with palladium but did not find penta-coordinate isomers; instead, we found only square-planar complexes. In a further attempt to optimize a penta-coordinate, we optimized a square-pyramidal geometry with a triflate in the apex. However, this led to the square-planar **1'** and a far distant triflate anion (>3 Å). The ionization of $[\text{Pd}(\text{CH}_2\text{CMe}_2\text{Ph})(\text{OTf})(\text{DMPE})]$ in dichloromethane solution into the corresponding **1'** cation and triflate is favorable by -6.7 Kcal/mol, which is close to the equivalent process for the square-planar nickel complexes (i.e., $-0.5 + (-5.7) = -6.2$ Kcal/mol). Note that, in addition to the internal π -arene interaction, these free energy balances include various other terms, such as the triflate-covalent bond, the electrostatic energy, and steric repulsive forces. Therefore, they cannot be taken as representative of the benzene ring π -binding energy.

A different structural problem that we found in our computational model concerns the structure of the binuclear hydroxide (**5a'**). As mentioned before, the crystal structure of the DiPPE-containing binuclear hydroxide **5a** has been reported in the literature [46]. In the solid state, the dication $[\text{Ni}(\mu\text{-OH})(\text{DiPPE})]_2^{2+}$ exhibits a flat $\text{Ni}_2(\mu\text{-OH})_2$ core, both in the triflate and PF_6^- salts. However, our initial calculations predicted a puckered four-membered Ni_2O_2 ring with a pronounced folding angle of 234.3° . This is expected if the bridging oxygen uses sp^3 hybrid orbitals with internal angles of ca. 109° . Yet, flat rings (i.e., with a dihedral angle close to 180°) are a common structural feature in the crystal structures of binuclear, hydroxyl-bridged complexes. A search in the Cambridge Structural Database [56] for binuclear Ni(II) hydroxides with phosphine ligands led to six hits, only one of which (CSD code FAYWAG) deviates significantly from planarity, with a 218° angle [57]. The same paper also reports on a close analog with a planar structure (CSD code FAYTIL). A careful inspection of these two structures shows that the hydroxyl hydrogen atoms in these compounds are in different conformations: on the same side of the Ni_2O_2 ring in FAYWAG and one on each side in FAYTIL. Extending our search to the heavier elements of group 10 led to a total of 33 hits (excluding redundant structures), 28 showing a planar M_2O_2 core, and only 5 having some significant folding. A problem with X-ray data is that, usually, H atoms are not accurately located in the electron density map. Old structures do not even include the hydrogen atom coordinates. When they do, H atoms are allowed to “ride” in a fixed position on their supporting atoms in the refining procedure. For this reason, it cannot be trusted that planar $\text{M}_2(\mu\text{-OH})_2$ cores are a real feature. In fact, the hydroxyl H atoms were located on opposite sides of the M_2O_2 ring in three “angular” structures (LEJGUF, REDZIJ, YUNBOY) and none on the same side. Thus, it seems that the angular configuration occasionally observed in binuclear hydroxides of this class probably corresponds with a cisoid disposition of the hydroxyl groups. Accordingly,

we set to model both *cis* and *trans* configurations for the hypothetical (not yet reported) dication $[\text{Ni}(\mu\text{-OH})(\text{DMPE})]^+$, and the calculations converged in two configurations, *cisoid* with the above-mentioned angular Ni_2O_2 ring and *transoid*, where this is essentially flat (Figure 3). The SCF energy favors the angular configuration by 6.7 Kcal/mol at the theory level used in geometry optimization. Still, it gives the opposite result in the high-level single-point calculation (the flat Ni_2O_2 ring being favored by 4.2 Kcal/mol). In terms of free energy, both conformers have nearly the same energy (just 0.4 Kcal/mol difference in favor of the angular), which suggests that the structure is flexible. Either configuration can be selected during the crystal growth process. In our final data, we always refer to the most stable configuration, which happens to be different for Pd, where the flat *transoid* conformer is favored by about one Kcal/mol.

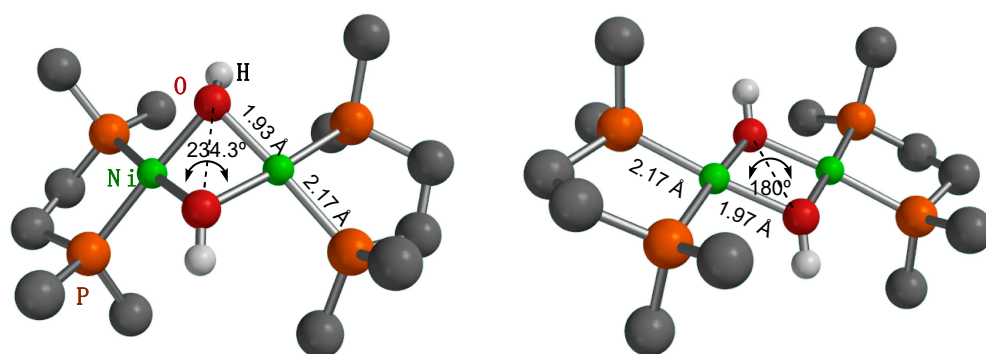


Figure 3. Two optimized geometries for the cation $[\text{Ni}(\mu\text{-OH})(\text{DMPE})]^+$ (**5a'**). The left side is the *cisoid* OH arrangement, with a pucker in the Ni_2O_2 ring; the right is the *transoid* with a flat Ni_2O_2 ring. Bond distances are nearly the same in both configurations. All hydrogen atoms, except for those of the OH groups, have been suppressed for clarity.

Once the main features of our model were addressed, we were ready to compare the feasibility of β -Ph elimination in Pd and Ni complexes. Given the prevalence of π -arene cations **1'** and **6'**, we can omit the triflate anion from this study and focus on discrete cationic species. The results are summarized in the free-energy profile diagram shown in Figure 4. The profiles for Ni and Pd include the hydrolysis of the putative 14-electron phenyl complexes, even though the second part of the reaction was never experimentally observed for palladium.

The initial part of the mechanism corresponds to the β -Ph elimination. To access the phenyl transfer transition state **TS1** from the π -arene species, the metal atom merely shifts from its π -arene coordination to interact with the σ - $\text{H}_2\text{C}-\text{CMe}_2(\text{Ph})$ bond. In the course of this process, the $\text{Me}_2\text{C}-\text{Ph}$ bond weakens, while the vicine $\text{Me}_2\text{C}-\text{CH}_2$ fragment becomes a coordinated isobutene molecule. As can be seen, this process is mildly endergonic, somewhat more so for nickel than for palladium. However, the energy barrier is substantially lower for Ni (18.2 Kcal/mol) than for palladium (23.9 Kcal/mol). These figures are consistent with the experiment: whereas **1** is relatively stable in solution, stirred suspensions of **6a** and **6b** decompose spontaneously at room temperature.

As discussed in the introduction, β -Ph elimination can be seen as the reverse of a migratory insertion of the isobutene ligand into the M-Ph bond. Since the phenyl-alkene products have similar stability (Pd, 8.7 vs. Ni, 7.7 vs. Kcal/mol, relative to the π -arenes **1'** and **6'**), the energy barrier in the backward direction (namely, the free energy difference between **TS1** and the phenyl-alkene complexes) is also smaller for Ni than for Pd. This is in keeping with many experimental and theoretical studies, which regularly report insertion barriers 4–5 Kcal/mol lower for Ni than for Pd. Most likely, the relative height of the energy barriers arises because the intermediates on both sides of **TS1** are better stabilized by their π -ligands for Pd than for Ni [58]. This is a consequence of the efficient overlapping of the carbon π orbitals by the 4d orbitals of Pd, compared to the more compact 3d shell of Ni [59].

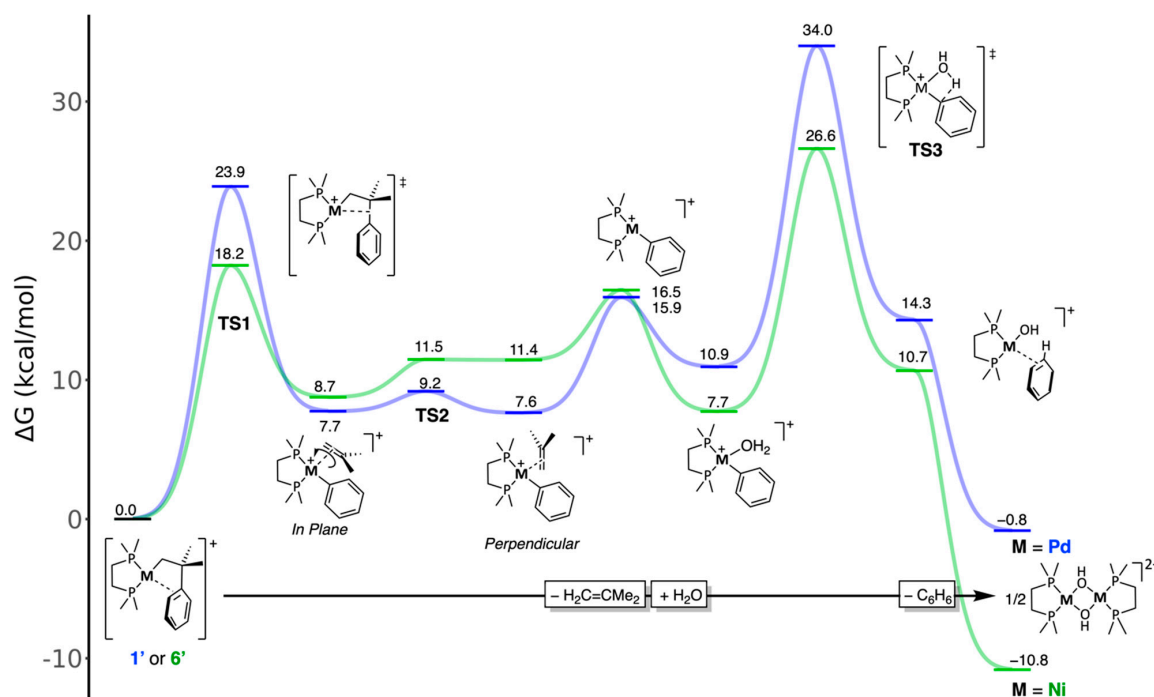


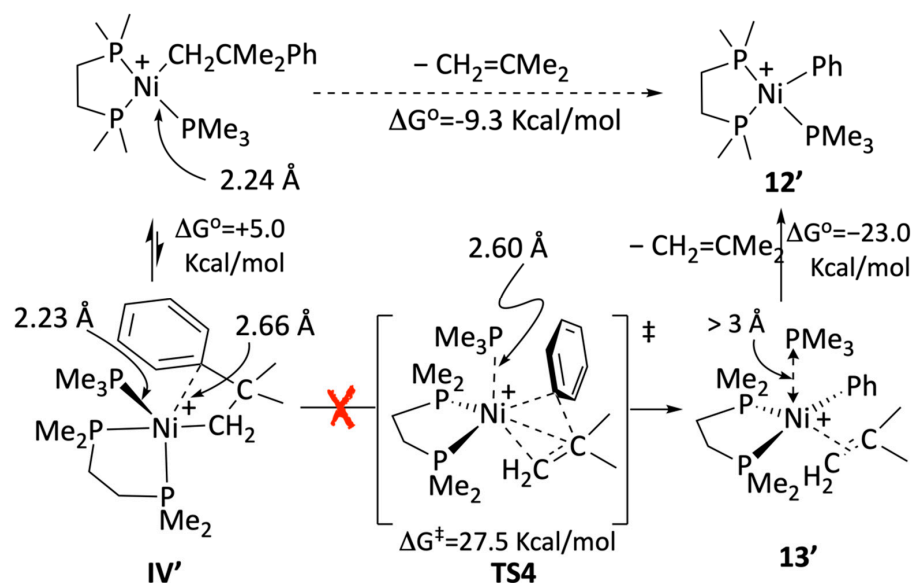
Figure 4. Free-energy profiles for the β -Ph elimination from the analogous π -arene model complexes **1'** (Pd) and **6'** (Ni). Free energy differences (in Kcal/mol) are shown for each intermediate or transition state, relative to the starting π -arene complexes plus/minus the contributions of the small molecules (isobutene, water, or benzene), as required according to the reaction stoichiometry.

Because the metal and the incipient phenyl and alkene ligands must be coplanar in the transition state **TS1**, the π -alkene ligand arises from this step in the “in-plane” conformation. It is known that 16-electron square planar complexes favor an “orthogonal” disposition of the alkene with regard to the ML_3 fragment, as in Zeise’s salt [60,61]. Thus, one would assume that the next logical step in this process is the rotation of the alkene to adopt the latter configuration. However, the situation turns out to be quite different for Ni and Pd. In the latter case, a facile rotation step ensues through the transition state **TS2**, leading to the slightly more stable π -alkene isomer. However, in the more crowded coordination sphere of the smaller Ni atom, the configuration of the “in-plane” isomer is distorted by steric repulsions, forcing the bulky isobutene to rotate out of the coordination plane. An “orthogonal” ground state still exists, but its structure and energy are very similar to those of **TS2**. The free energy of this transition state is estimated to be very close to that of the orthogonal product (see Computational Details in the Materials and Methods Section), meaning that the orthogonal π -isobutene ligand is destabilized in the Ni system, favoring its release. In fact, including the entropy for alkene dissociation, the coordinatively unsaturated phenyl species $[Ni(Ph)(DMPE)]^+$ lies only 5 Kcal/mol above the latter isomer. For palladium, isobutene dissociation is considerably more endergonic (+8.6 Kcal/mol). Both highly reactive 14-electron $[M(Ph)(DMPE)]^+$ fragments can then be trapped by a water molecule as the aqua complexes [62] $[M(Ph)(H_2O)(DMPE)]$. A water molecule stabilizes the Ni intermediate more efficiently than its Pd counterpart (by 8.8 vs. 5.0 Kcal/mol), preconfiguring a more facile hydrolytic pathway for Ni. Substituting the isobutene ligand with water might also involve an associative process [63,64]. However, we have not explored this pathway, since water is a trace impurity in our system. This aspect of the mechanism is not critical, since the exchange of the π -olefin ligand is, in terms of free energy, moderately downhill along the nickel profile and considerably uphill in the case of Pd. This pre-configures the different hydrolytic behavior of Ni and Pd once the β -Ph step has taken place.

Next, the aqua intermediates undergo intramolecular proton transfer from the coordinated water to the phenyl ligand, leading to monomeric hydroxide complexes stabilized by a π -coordinated benzene ligand. This can be seen as an intramolecular electrophilic attack on the metal-bound carbon atom from the aqua ligand, whose acidity is enhanced by the positively charged metal. This view is supported by the resistance of complexes such as $[\text{Ni}(\text{Me})(\text{Py})(\text{DiPPE})]^+$ to hydrolysis since the sp^3 hybridized methyl carbon atom is less amenable to electrophilic attack. The transition state **TS3**, corresponding to the $\text{X}\cdots\text{H}\cdots\text{C}$ proton transfer, leads to a monomeric hydroxide stabilized by a π -benzene ligand, which is readily lost in a strongly exergonic step to yield the final binuclear hydroxides. **TS3** is similar to that found in the 1,2-C-H addition to M-OR or M-OH bonds, described by Cundari and Gunnoe for Ru complexes [65] and more recently investigated by Schafer and Love for Ni [66]. The free energy barrier to the proton transfer from the aqua precursor is considerably higher for Pd (22.4 Kcal/mol) than for Ni (18.9 Kcal/mol). The different energies of **TS3** in the Ni and Pd profiles of the hydrolysis reaction can be rationalized, considering that it involves the formation of a covalent M-OH linkage at the expense of an M-C bond. We have shown in a previous contribution [67] that the Ni-OH bond is stronger than the Pd-OH because of the dipolar contribution from the electrostatic attraction between the compact-sized OH ligand and the smaller metal cation. A similar explanation could also be invoked for the more efficient stabilization of Ni species by water compared to Pd. Overcoming the whole barrier is only feasible for the former (26.9 vs. 34.3 Kcal/mol). Accordingly, no hydrolysis products were formed when the decomposition of complex **1** was thermally induced in the absence of **3**. Only isobutene, some Pd black, and ill-defined products were observed [39].

As mentioned previously, 16-electron neophyl nickel complexes, such as the pyridine adduct **7a** or its putative PMe_3 analog, also undergo facile β -Ph elimination, even at room temperature, with no need for a catalytic amount of a cationic catalyst such as **6a**. This could suggest the possibility of a more direct pathway to β -Ph elimination, operating through a pentacoordinate intermediate of type **IV** in this case. Given its potential interest in nickel-catalyzed reactions, we have also modeled this route. Interestingly, the conformational analyses of the 16-electron neophyl intermediate $[\text{Ni}(\text{CH}_2\text{CMe}_2\text{Ph})(\text{PMe}_3)(\text{DMPE})]^+$ revealed the existence of a stable pentacoordinate isomer, **IV'**, lying only 5 Kcal/mol above its square-planar isomer (Scheme 8). Similar interactions have been experimentally discovered in nickel phosphinoenolato complexes with biphenyl substituents on the P atom [68].

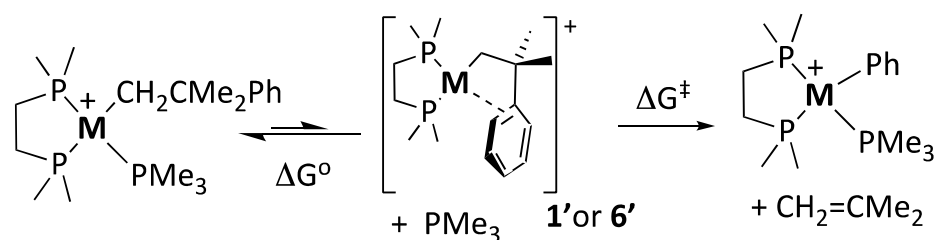
The intermediate **IV'** has an approximately trigonal bipyramidal geometry, with the PMe_3 and the π -arene ligands lying in the equatorial plane, while the CH_2 and one of the PMe_2 donor groups are positioned along the axis. Thus, the π -arene interaction, although weak, causes a noticeable distortion of the geometry of the Ni center. An 18-electron transition state, **TS4**, connects **IV'** with the corresponding phenyl-isobutene complex, **13'**. Interestingly, the Ni- PMe_3 interaction fades on going from **IV'** to **TS4** and then to **13'**, as reflected by the long Ni-P distances, 2.60 Å and more than 3 Å, respectively. The latter can be regarded as fully dissociated. Then, a facile exchange of the olefin ligand with the nearby PMe_3 would lead to the phenyl-phosphine product **12'**. We located the corresponding transition state, **TS5**, which is not shown in the scheme for simplicity (the free-energy profile is provided in the Supplementary Material, Figure S3). The whole process is exergonic by -9.3 Kcal/mol. Therefore, the direct non-dissociative mechanism is a possibility for β -Ph elimination. However, a closer examination of the mechanism shown in Scheme 8 indicates this is highly unlikely.



Scheme 8. Associative β -Ph elimination through the 18-electron intermediate **IV** without PMe_3 dissociation.

The main drawback of the above mechanism is the unrealistic high energy barrier (ΔG^\ddagger) that **TS4** poses to the β -Ph elimination from **IV'**. Assuming that the 16-electron neophyl- PMe_3 complex is in equilibrium with **IV'**, the overall barrier would be $27.5 + 5.0 = 32.5$ Kcal/mol, which is not accessible at room temperature. Notice that the reversal, i.e., associative carbometallation, is even less likely (this is best appreciated in Figure S3). This is mainly due to the prohibitive energy cost of temporarily displacing PMe_3 with such a poor ligand as isobutene.

As an alternative, we investigated the feasibility of a dissociative mechanism involving the initial release of a PMe_3 ligand. For this purpose, it is helpful to consider the dissociative equilibria shown in Scheme 9.



M	$\Delta E_{(\text{SCF}+\text{ZPE})}$	ΔG°	ΔG^\ddagger	$\Delta G^\circ + \Delta G^\ddagger$
Ni	19.8	2.3	18.2	20.5
Pd	23.6	6.4	23.9	30.2

Scheme 9. Computed free energy barriers ($\Delta G^\circ + \Delta G^\ddagger$, Kcal/mol) for the dissociative β -Ph elimination reactions with **M** = Ni and Pd.

As can be seen, this mechanism involves the displacement of the monodentate PMe_3 ligand by the phenyl fragment of the alkyl. The reaction heat (represented here by the conceptually more accurate zero-point-corrected energy balance, $\Delta E_{\text{SCF}+\text{ZPE}}$) is strongly endothermic. However, the entropy contribution due to the release of PMe_3 ligand offsets the unfavorable energy change, and the dissociation is mildly endergonic. For Ni, PMe_3 dissociation is further favored by the weaker ligand bonding in the $3d$ series and by the

strain release due to the small size of the Ni atom. The latter is probably more acute with the bulkier diphosphine DiPP used in the experiment.

Assuming that the phosphine dissociation that leads to the π -arene intermediate is a fast equilibrium, its free energy variation (ΔG°) adds to the energy barrier for the rate-limiting β -Ph elimination (ΔG^\ddagger) to compose the actual energy barrier for the whole elimination process, as shown in Scheme 9. In agreement with our experimental observations, the overall barrier ($\Delta G^\circ + \Delta G^\ddagger$) is too high for the Pd complex (30.2 Kcal/mol). For Ni, it is only 20.5 Kcal/mol, low enough to assume a spontaneous reaction at a mild temperature. Moreover, the availability of the five-coordinated species **IV'** indicates that PMe_3 could be displaced through an intramolecular "associative" mechanism rather than undergoing spontaneous dissociation. The energy barrier for the Ni preequilibrium would be only slightly above that of **IV'** (≈ 5 Kcal/mol). On the contrary, we could not locate a pentacoordinate intermediate or a similar intramolecular transition state to access **1'**; we are forced to believe that direct dissociation of PMe_3 would be required to enable β -Ph elimination from the Pd complex. Even if this difficulty is neglected, the composed barrier would be too high at room temperature, which explains the experimentally observed need to bait the PMe_3 complex $[\text{PdCH}_2\text{CMe}_2\text{Ph}(\text{PMe}_3)(\text{DMPE})]$ (**3**) with a catalytic amount of **1** to enable a productive β -Ph reaction to proceed [39].

5. Conclusions

We have shown that, similar to their Pd counterparts, Ni-neophyl complexes are also prone to undergo irreversible transformations triggered by β -Ph elimination, the microscopic reverse of olefin migratory insertion into an M-Ph bond. Neophylnickel triflate complexes **5a** and **5b** containing a chelating diphosphine (DiPPE or DiPPP) were generated at low temperatures by protonating the metalacyclic precursors **4a** and **4b** with triflic acid. These complexes probably feature a π -arene interaction that promotes β -Ph elimination. Traces of water trap the resulting phenyl-nickel species to yield the binuclear hydroxo-bridged dimers **4a** and **4b**, which greatly facilitated the elucidation of the whole process.

The 16-electron neophylnickel cations of the type $[\text{Ni}(\text{CH}_2\text{CMe}_2\text{Ph})(\text{L})(\text{P-P})]^+$ (L = monodentate base) also undergo β -Ph elimination. The coordinating strength of the ancillary ligand L can modulate the stability of such complexes. A qualitative stability order, L = none < Py, PMe_3 < DMAP, emerges from these experiments. For L = Py or PMe_3 , the decomposition still occurs readily at room temperature, in contrast with the thermally stable Pd cation $[\text{Pd}(\text{CH}_2\text{CMe}_2\text{Ph})(\text{PMe}_3)(\text{DMPE})]^+$, previously reported by our group. This suggests that β -Ph elimination is kinetically easier for nickel neophyl derivatives than their Pd analogs.

DFT calculations support the above conclusions. A comparison of the β -Ph elimination step in the isostructural Pd and Ni DMPE models **1'** and **6'** draws a significantly lower barrier for the latter, even though the elimination step is somewhat more thermodynamically favorable for the former. While the instability of the square-planar 16-electron adducts of pyridine and PMe_3 suggested that phenyl abstraction, similar to β -H elimination, might proceed directly via a pentacoordinate transition state, this study has shown that the energy of this latter is prohibitively high. Instead, the dissociation of the ligand L (presumably assisted by the phenyl fragment) does explain our experimental observations. Since β -Ph elimination is the microscopic reverse of olefin carbometallation, the latter conclusion is in line with the dearth of literature examples of direct carbometallation via five-coordinated transition states.

An additional lesson to be learned from this study is that nickel complexes are often more sensitive to hydrolytic decay compared to their palladium counterparts. The facile trapping of the phenyl-Ni species by water results from the stronger Ni-OH bond and the relatively facile intramolecular H transfer from a coordinated aqua complex to the Ni-bound Ph, whose energy barrier is significantly higher for palladium. The facile hydrolysis of nickel-aryl complexes suggests that strict anhydrous conditions may prove more critical

for catalytic applications of nickel compounds, particularly those involving nickel catalysts in cationic Mizoroki–Heck reactions.

Supplementary Materials: The following supplementary information can be downloaded at <https://www.mdpi.com/article/10.3390/inorganics12030089/s1>, Computational results showing the energy of π -arene interactions in isostructural Ni-neophyl complexes with DMPE, DiPPE and DtBPE, conformational isomers of neophyl-triflate complexes, energy component breakdown for all stationary points located in the β -Ph elimination and hydrolyses reactions of Ni and Pd neophyl species, and molecular drawings and atomic coordinates for all optimized geometries.

Author Contributions: J.A.L. and D.A.C., experimental research and data organization and collection; P.P., supervision, writing, review, and project administration. J.C., supervision, conceptualization, computational work, writing, and review. All authors have read and agreed to the published version of the manuscript.

Funding: This research was supported by the European Union (Feder Funds), the Spanish Research Agency (AEI) and Junta de Andalucía, through projects PID2021–128392NB–100 and P20_00104, respectively.

Data Availability Statement: Spectral data and plots, and other materials supporting this article are available from the corresponding author upon reasonable request.

Acknowledgments: D.A.C. thanks a Ph.D. training grant (PRE2019-087770) from the AEI and the European Social Fund.

Conflicts of Interest: The authors declare no conflicts of interest.

References

1. Hartwig, J.F. Chapters 9, Migratory Insertion Reactions, and 10, Elimination Reactions. In *Organotransition Metal Chemistry, from Bonding to Catalysis*; University Science Books: Sausalito, CA, USA, 2010; pp. 349–416.
2. Wilke, G. Karl Ziegler—The Last Alchemist. In *Ziegler Catalysts: Recent Scientific Innovations and Technological Improvements*; Ziegler, K., Fink, G., Mülhaupt, R., Brintzinger, H.H., Eds.; Springer: Berlin/Heidelberg, Germany, 1995; pp. 1–14.
3. Brintzinger, H.H.; Fischer, D.; Mülhaupt, R.; Rieger, B.; Waymouth, R.M. Stereospecific Olefin Polymerization with Chiral Metallocene Catalysts. *Angew. Chem. Int. Ed. Engl.* **1995**, *34*, 1143–1170. [[CrossRef](#)]
4. Coates, G.W. Precise Control of Polyolefin Stereochemistry Using Single-Site Metal Catalysts. *Chem. Rev.* **2000**, *100*, 1223–1252. [[CrossRef](#)]
5. Ittel, S.D.; Johnson, L.K.; Brookhart, M. Late-Metal Catalysts for Ethylene Homo- and Copolymerization. *Chem. Rev.* **2000**, *100*, 1169–1204. [[CrossRef](#)]
6. Bochmann, M. Kinetic and mechanistic aspects of metallocene polymerisation catalysts. *J. Organomet. Chem.* **2004**, *689*, 3982–3998. [[CrossRef](#)]
7. Ewen, J.A. Mechanisms of stereochemical control in propylene polymerizations with soluble Group 4B metallocene/methylalumoxane catalysts. *J. Am. Chem. Soc.* **1984**, *106*, 6355–6364. [[CrossRef](#)]
8. Coates, G.W.; Waymouth, R.M. Oscillating Stereocontrol: A Strategy for the Synthesis of Thermoplastic Elastomeric Polypropylene. *Science* **1995**, *267*, 217–219. [[CrossRef](#)] [[PubMed](#)]
9. Johnson, L.K.; Killian, C.M.; Brookhart, M. New Pd(II)- and Ni(II)-Based Catalysts for Polymerization of Ethylene and α -Olefins. *J. Am. Chem. Soc.* **1995**, *117*, 6414–6415. [[CrossRef](#)]
10. Svejda, S.A.; Johnson, L.K.; Brookhart, M. Low-Temperature Spectroscopic Observation of Chain Growth and Migratory Insertion Barriers in (α -Diimine)Ni(II) Olefin Polymerization Catalysts. *J. Am. Chem. Soc.* **1999**, *121*, 10634–10635. [[CrossRef](#)]
11. Tempel, D.J.; Johnson, L.K.; Huff, R.L.; White, P.S.; Brookhart, M. Mechanistic Studies of Pd(II)– α -Diimine-Catalyzed Olefin Polymerizations I. *J. Am. Chem. Soc.* **2000**, *122*, 6686–6700. [[CrossRef](#)]
12. Leatherman, M.D.; Svejda, S.A.; Johnson, L.K.; Brookhart, M. Mechanistic Studies of Nickel(II) Alkyl Agostic Cations and Alkyl Ethylene Complexes: Investigations of Chain Propagation and Isomerization in (α -diimine)Ni(II)-Catalyzed Ethylene Polymerization. *J. Am. Chem. Soc.* **2003**, *125*, 3068–3081. [[CrossRef](#)]
13. Keim, W. Oligomerization of Ethylene to α -Olefins: Discovery and Development of the Shell Higher Olefin Process (SHOP). *Angew. Chem. Int. Ed.* **2013**, *52*, 12492–12496. [[CrossRef](#)] [[PubMed](#)]
14. Speiser, F.; Braunstein, P.; Saussine, L. Catalytic Ethylene Dimerization and Oligomerization: Recent Developments with Nickel Complexes Containing P,N-Chelating Ligands. *Acc. Chem. Res.* **2005**, *38*, 784–793. [[CrossRef](#)] [[PubMed](#)]
15. Small, B.L. Discovery and Development of Pyridine-bis(imine) and Related Catalysts for Olefin Polymerization and Oligomerization. *Acc. Chem. Res.* **2015**, *48*, 2599–2611. [[CrossRef](#)]
16. Bekmukhamedov, G.E.; Sukhov, A.V.; Kuchkaev, A.M.; Yakhvarov, D.G. Ni-Based Complexes in Selective Ethylene Oligomerization Processes. *Catalysts* **2020**, *10*, 498. [[CrossRef](#)]

17. Olivier-Bourbigou, H.; Breuil, P.A.R.; Magna, L.; Michel, T.; Espada Pastor, M.F.; Delcroix, D. Nickel Catalyzed Olefin Oligomerization and Dimerization. *Chem. Rev.* **2020**, *120*, 7919–7983. [[CrossRef](#)] [[PubMed](#)]
18. Keim, W.; Behr, A.; Gruber, B.; Hoffmann, B.; Kowaldt, F.H.; Kuerschner, U.; Limbaecker, B.; Sistig, F.P. Reactions of chelate ylides with nickel(0) complexes. *Organometallics* **1986**, *5*, 2356–2359. [[CrossRef](#)]
19. Hasanayn, F.; Achord, P.; Braunstein, P.; Magnier, H.J.; Krogh-Jespersen, K.; Goldman, A.S. Theoretical Structure–Reactivity Study of Ethylene Insertion into Nickel–Alkyl Bonds. A Kinetically Significant and Unanticipated Role of trans Influence in Determining Agostic Bond Strengths. *Organometallics* **2012**, *31*, 4680–4692. [[CrossRef](#)]
20. Beletskaya, I.P.; Cheprakov, A.V. The Heck Reaction as a Sharpening Stone of Palladium Catalysis. *Chem. Rev.* **2000**, *100*, 3009–3066. [[CrossRef](#)]
21. Bhakta, S.; Ghosh, T. Emerging Nickel Catalysis in Heck Reactions: Recent Developments. *Adv. Synth. Catal.* **2020**, *362*, 5257–5274. [[CrossRef](#)]
22. Anslyn, E.V.; Dougherty, D.A. *Modern Physical Organic Chemistry*; University Science Books: Mill Valley, CA, USA, 2006.
23. O'Reilly, M.E.; Dutta, S.; Veige, A.S. β -Alkyl Elimination: Fundamental Principles and Some Applications. *Chem. Rev.* **2016**, *116*, 8105–8145. [[CrossRef](#)]
24. Martinho-Simoes, J.A.M.; Beauchamp, J.L. Transition metal-hydrogen and metal-carbon bond strengths: The keys to catalysis. *Chem. Rev.* **1990**, *90*, 629–688. [[CrossRef](#)]
25. Shirasawa, N.; Nguyet, T.T.; Hikichi, S.; Moro-oka, Y.; Akita, M. Tetrahedral, Highly Coordinatively Unsaturated 14e (Fe) and 15e (Co) Hydrocarbyl Complexes Bearing Hydrotris(pyrazolyl)borato Ligands (TpR'), TpR'M–R (M = Fe, Co, Ni). *Organometallics* **2001**, *20*, 3582–3598. [[CrossRef](#)]
26. Matas, I.; Cámpora, J.; Palma, P.; Álvarez, E. Decomposition of Methylnickel(II) Amido, Alkoxo, and Alkyl Complexes by β -Hydrogen Elimination: A Comparative Study. *Organometallics* **2009**, *28*, 6515–6523. [[CrossRef](#)]
27. Vela, J.; Vaddadi, S.; Cundari, T.R.; Smith, J.M.; Gregory, E.A.; Lachicotte, R.J.; Flaschenriem, C.J.; Holland, P.L. Reversible Beta-Hydrogen Elimination of Three-Coordinate Iron(II) Alkyl Complexes: Mechanistic and Thermodynamic Studies. *Organometallics* **2004**, *23*, 5226–5239. [[CrossRef](#)]
28. Brown, J.M.; Hii, K.K. Characterization of Reactive Intermediates in Palladium-Catalyzed Arylation of Methyl Acrylate (Heck Reaction). *Angew. Chem. Int. Ed. Engl.* **1996**, *35*, 657–659. [[CrossRef](#)]
29. Carr, N.; Mole, L.; Orpen, A.G.; Spencer, J.L. Platinum ethyl complexes with β -agostic Pt–H–C bonding. *J. Chem. Soc. Dalton Trans.* **1992**, 2653–2662. [[CrossRef](#)]
30. Conroy-Lewis, F.M.; Mole, L.; Redhouse, A.D.; Litster, S.A.; Spencer, J.L. Synthesis of coordinatively unsaturated diphosphine nickel(II) and palladium(II) β -agostic ethyl cations: X-ray crystal structure of $[\text{Ni}\{\text{But}_2\text{P}(\text{CH}_2)_2\text{Pbut}_2\}(\text{C}_2\text{H}_5)][\text{BF}_4]$. *J. Chem. Soc. Chem. Commun.* **1991**, 1601–1603. [[CrossRef](#)]
31. Etienne, M.; Weller, A.S. Intramolecular C–C agostic complexes: C–C sigma interactions by another name. *Chem. Soc. Rev.* **2014**, *43*, 242–259. [[CrossRef](#)]
32. Sini, G.; Macgregor, S.A.; Eisenstein, O.; Teuben, J.H. Why Is β -Me Elimination Only Observed in d^0 Early-Transition-Metal Complexes? An Organometallic Hyperconjugation Effect with Consequences for the Termination Step in Ziegler-Natta Catalysis. *Organometallics* **1994**, *13*, 1049–1051. [[CrossRef](#)]
33. Samudrala, K.K.; Conley, M.P. A Supported Ziegler-Type Organohafnium Site Metabolizes Polypropylene. *J. Am. Chem. Soc.* **2023**, *145*, 24447–24451. [[CrossRef](#)] [[PubMed](#)]
34. Le Bras, J.; Muzart, J. β -Elimination competitions leading to CC bonds from alkylpalladium intermediates. *Tetrahedron* **2012**, *68*, 10065–10113. [[CrossRef](#)]
35. Wang, J.; Dong, G. Palladium/Norbornene Cooperative Catalysis. *Chem. Rev.* **2019**, *119*, 7478–7528. [[CrossRef](#)]
36. Amatore, C.; Godin, B.; Jutand, A.; Lemaître, F. Rate and Mechanism of the Heck Reactions of Arylpalladium Complexes Ligated by a Bidentate P,P Ligand with an Electron-Rich Alkene (Isobutyl Vinyl Ether). *Organometallics* **2007**, *26*, 1757–1761. [[CrossRef](#)]
37. Cámpora, J.; López, J.A.; Palma, P.; Valerga, P.; Spillner, E.; Carmona, E. Cleavage of Palladium Metallacycles by Acids: A Probe for the Study of the Cyclometalation Reaction. *Angew. Chem. Int. Ed.* **1999**, *38*, 147–151. [[CrossRef](#)]
38. Catellani, M.; Mealli, C.; Motti, E.; Paoli, P.; Perez-Carreño, E.; Pregosin, P.S. Palladium–Arene Interactions in Catalytic Intermediates: An Experimental and Theoretical Investigation of the Soft Rearrangement between η^1 and η^2 Coordination Modes. *J. Am. Chem. Soc.* **2002**, *124*, 4336–4346. [[CrossRef](#)] [[PubMed](#)]
39. Cámpora, J.; Gutiérrez-Puebla, E.; López, J.A.; Monge, A.; Palma, P.; del Río, D.; Carmona, E. Cleavage of the $\text{C}_{\text{alkyl}}-\text{C}_{\text{aryl}}$ Bond of $[\text{Pd}-\text{CH}_2\text{Cme}_2\text{Ph}]$ Complexes. *Angew. Chem. Int. Ed.* **2001**, *40*, 3641–3644. [[CrossRef](#)]
40. Thorn, D.L.; Hoffmann, R. The olefin insertion reaction. *J. Am. Chem. Soc.* **1978**, *100*, 2079–2090. [[CrossRef](#)]
41. Gallazzi, M.C.; Porri, L.; Vitulli, G. Reversible insertion of norbornene into a nickel methallyl bond. *J. Organomet. Chem.* **1975**, *97*, 131–138. [[CrossRef](#)]
42. Van der Boom, M.E.; Liou, S.-Y.; Shimon, L.J.W.; Ben-David, Y.; Milstein, D. Nickel promoted C–H, C–C and C–O bond activation in solution. *Inorganica Chim. Acta* **2004**, *357*, 4015–4023. [[CrossRef](#)]
43. Cámpora, J.; López, J.A.; Maya, C.; Palma, P.; Carmona, E.; Valerga, P. Synthesis and reactivity studies on alkyl-aryloxo complexes of nickel containing chelating diphosphines: Cyclometallation and carbonylation reactions. *J. Organomet. Chem.* **2002**, *643–644*, 331–341. [[CrossRef](#)]

44. Deppmeier, B.; Drissen, A.; Hehre, T.; Hehre, W.; Kluzinger, P.; Ohlinger, S.; Schnitker, J. *Spartan'20, Version 1.1.4*; Wavefunction, Inc.: Irvine, CA, USA, 2021.
45. Bogdos, M.K.; Morandi, B. EveRplot: A Web-Based Shiny Application for Creating Energy vs Reaction Coordinate Diagrams. *J. Chem. Ed.* **2023**, *100*, 3641–3644. [[CrossRef](#)]
46. Morales-Becerril, I.; Flores-Álamo, M.; Tlahuext-Aca, A.; Arévalo, A.; García, J.J. Synthesis of Low-Valent Nickel Complexes in Aqueous Media, Mechanistic Insights, and Selected Applications. *Organometallics* **2014**, *33*, 6796–6802. [[CrossRef](#)]
47. Cámpora, J.; Palma, P.; Carmona, E. The chemistry of group 10 metalacycles. *Coord. Chem. Rev* **1999**, *193–195*, 207–281. [[CrossRef](#)]
48. Cámpora, J.; López, J.A.; Palma, P.; del Rio, D.; Carmona, E.; Valerga, P.; Graiff, C.; Tiripicchio, A. Synthesis and Insertion Reactions of the Cyclometalated Palladium–Alkyl Complexes Pd(CH₂Cme₂–o–C₆H₄)L₂. Observation of a Pentacoordinated Intermediate in the Insertion of SO₂. *Inorg. Chem.* **2001**, *40*, 4116–4126. [[CrossRef](#)] [[PubMed](#)]
49. Ortiz de la Tabla, L.; Matas, I.; Álvarez, E.; Palma, P.; Cámpora, J. Migratory insertion reactions of nickel and palladium σ -alkyl complexes with a phosphinito-imine ligand. *Dalton Trans.* **2012**, *41*, 14524–14539. [[CrossRef](#)]
50. Cámpora, J.; Conejo, M.M.; Mereiter, K.; Palma, P.; Pérez, C.; Reyes, M.L.; Ruiz, C. Synthesis of dialkyl, diaryl and metallacyclic complexes of Ni and Pd containing pyridine, α -diimines and other nitrogen ligands: Crystal structures of the complexes *cis*-NiR₂py₂ (R=benzyl, mesityl). *J. Organomet. Chem.* **2003**, *683*, 220–239. [[CrossRef](#)]
51. Kitiachvili, K.D.; Mindiola, D.J.; Hillhouse, G.L. Preparation of Stable Alkyl Complexes of Ni(I) and Their One-Electron Oxidation to Ni(II) Complex Cations. *J. Am. Chem. Soc.* **2004**, *126*, 10554–10555. [[CrossRef](#)] [[PubMed](#)]
52. Hernández, J.; Muller, G.; Rocamora, M.; Solans, X.; Aguiló, M. Reactions of activated alkynes with organonickel complexes. Crystal structure of *trans*-[NiBr(C(COOMe)=C(COOMe) (3,5-Cl₂C₆H₃))(PPh₃)₂]. *J. Organomet. Chem.* **1988**, *345*, 383–396. [[CrossRef](#)]
53. Ceder, R.M.; Cubillo, J.; Muller, G.; Rocamora, M.; Sales, J. Reactions of neutral and ionic square-planar organometallic nickel compounds with ethylene. *J. Organomet. Chem.* **1992**, *429*, 391–401. [[CrossRef](#)]
54. Cámpora, J.; Conejo, M.M.; Reyes, M.L.; Mereiter, K.; Passaglia, E. η^6 -Arene complexes of Ni(II), efficient catalysts for 1,3-butadiene and styrene polymerization. *Chem. Commun.* **2003**, 78–79. [[CrossRef](#)]
55. Walter, M.D.; Moorhouse, R.A.; White, P.S.; Brookhart, M. Vinyl addition polymerization of norbornene with cationic (allyl)Ni catalysts: Mechanistic insights and characterization of first insertion products. *J. Polym. Sci. A. Polym. Chem.* **2009**, *47*, 2560–2573. [[CrossRef](#)]
56. *Cambridge Structural Database (CSD)*, version 5.43 (November 2021); 12 Union Road, Cambridge CB2 1EZ, United Kingdom. Searched with the CCDC ConQuest software, Version 2022.3.0; The Cambridge Crystallographic Data Centre (CCDC): Cambridge, UK, 2021.
57. Lee, K.; Donahue, C.M.; Daly, S.R. Triaminoborane-bridged diphosphine complexes with Ni and Pd: Coordination chemistry, structures, and ligand-centered reactivity. *Dalton Trans.* **2017**, *46*, 9394–9406. [[CrossRef](#)] [[PubMed](#)]
58. Rix, F.C.; Brookhart, M.; White, P.S. Electronic Effects on the β -Alkyl Migratory Insertion Reaction of *para*-Substituted Styrene Methyl Palladium Complexes. *J. Am. Chem. Soc.* **1996**, *118*, 2436–2448. [[CrossRef](#)]
59. Frenking, G.; Fröhlich, N. The Nature of the Bonding in Transition-Metal Compounds. *Chem. Rev.* **2000**, *100*, 717–774. [[CrossRef](#)]
60. Strömberg, S.; Svensson, M.; Zetterberg, K. Binding of Ethylene to Anionic, Neutral, and Cationic Nickel(II), Palladium(II), and Platinum(II) *cis/trans* Chloride Ammonia Complexes. A Theoretical Study. *Organometallics* **1997**, *16*, 3165–3168. [[CrossRef](#)]
61. Forniés, J.; Martín, A.; Martín, L.F.; Menjón, B.; Tsiapis, A. All-Organometallic Analogues of Zeise's Salt for the Three Group 10 Metals. *Organometallics* **2005**, *24*, 3539–3546. [[CrossRef](#)]
62. Vicente, J.; Arcas, A. Aqua palladium complexes: Synthesis, properties and applications. *Coord. Chem. Rev* **2005**, *249*, 1135–1154. [[CrossRef](#)]
63. Casares, J.A.; Espinet, P.; Martín-Alvarez, J.M.; Martínez-Ilarduya, J.M.; Salas, G. Stable Nickel Catalysts for Fast Norbornene Polymerization: Tuning Reactivity. *Eur. J. Inorg. Chem.* **2005**, *2005*, 3825–3831. [[CrossRef](#)]
64. Casares, J.A.; Espinet, P.; Martínez-Ilarduya, J.M.; Mucientes, J.J.; Salas, G. Study of the Replacement of Weak Ligands on Square-Planar Organometallic Nickel(II) Complexes. Organo-Nickel Aquacomplexes. *Inorg. Chem.* **2007**, *46*, 1027–1032. [[CrossRef](#)]
65. Webb, J.R.; Burgess, S.A.; Cundari, T.R.; Gunnoe, T.B. Activation of carbon–hydrogen bonds and dihydrogen by 1,2-CH-addition across metal–heteroatom bonds. *Dalton Trans.* **2013**, *42*, 16646–16665. [[CrossRef](#)]
66. Beattie, D.D.; Grunwald, A.C.; Perse, T.; Schafer, L.L.; Love, J.A. Understanding Ni(II)-Mediated C(sp³)-H Activation: Tertiary Ureas as Model Substrates. *J. Am. Chem. Soc.* **2018**, *140*, 12602–12610. [[CrossRef](#)] [[PubMed](#)]
67. Martínez-Prieto, L.M.; Palma, P.; Álvarez, E.; Cámpora, J. Nickel Pincer Complexes with Frequent Aliphatic Alkoxy Ligands [(iPrPCP)Ni-OR] (R = Et, nBu, iPr, 2-hydroxyethyl). An Assessment of the Hydrolytic Stability of Nickel and Palladium Alkoxides. *Inorg. Chem.* **2017**, *56*, 13086–13099. [[CrossRef](#)] [[PubMed](#)]
68. Lin, F.; Voccia, M.; Odenwald, L.; Göttker-Schnetmann, I.; Falivene, L.; Caporaso, L.; Mecking, S. Origin of Suppressed Chain Transfer in Phosphinephenolato Ni(II)-Catalyzed Ethylene Polymerization. *J. Am. Chem. Soc.* **2023**, *145*, 27950–27957. [[CrossRef](#)] [[PubMed](#)]

Disclaimer/Publisher's Note: The statements, opinions and data contained in all publications are solely those of the individual author(s) and contributor(s) and not of MDPI and/or the editor(s). MDPI and/or the editor(s) disclaim responsibility for any injury to people or property resulting from any ideas, methods, instructions or products referred to in the content.